

Rates of Neutrino Absorption on Nucleons and the Reverse Processes in Strong Magnetic Fields

Huaiyu Duan* and Yong-Zhong Qian†

School of Physics and Astronomy, University of Minnesota, Minneapolis, MN 55455

(Dated: February 20, 2019)

The rates of $\nu_e + n \rightleftharpoons e^- + p$ and $\bar{\nu}_e + p \rightleftharpoons e^+ + n$ are important for understanding the production of heavy elements in the supernova environment above the protoneutron star. Observations and theoretical considerations suggest that some protoneutron stars may be born with strong magnetic fields. We develop a numerical method to calculate the above rates in supernova environments with magnetic fields up to $\sim 10^{16}$ G. This method is accurate to $\mathcal{O}(1/m_N)$ (m_N being the nucleon mass). We show that our results have the correct behavior in the limit of high neutrino energy or small magnetic field. Based on comparison of our results with various approximations, we recommend efficient estimates of the above rates for use in models of supernova nucleosynthesis in the presence of strong magnetic fields.

PACS numbers: 25.30.Pt, 26.50.+x, 97.60.Bw

I. INTRODUCTION

The processes

$$\nu_e + n \rightleftharpoons e^- + p, \quad (1a)$$

$$\bar{\nu}_e + p \rightleftharpoons e^+ + n, \quad (1b)$$

play important roles in supernovae. A supernova is initiated by the collapse of a stellar core, which leads to the formation of a protoneutron star. Nearly all the gravitational binding energy of the protoneutron star is emitted in ν_e , $\bar{\nu}_e$, ν_μ , $\bar{\nu}_\mu$, ν_τ , and $\bar{\nu}_\tau$, some of which would interact to heat the material above the protoneutron star. The forward neutrino absorption processes in Eq. (1) provide the dominant heating mechanism, which is counteracted by cooling of the material through the reverse neutrino emission processes. In a prevalent paradigm [1], supernova explosion is determined by the competition between these heating and cooling processes. These processes also interconvert neutrons and protons, thereby setting the neutron-to-proton ratio of the material above the protoneutron star [2]. This ratio is a key parameter that governs the production of heavy elements during the ejection of this material [3, 4]. Thus, accurate rates of the processes in Eq. (1) are important for understanding supernova dynamics and nucleosynthesis.

In this paper we calculate the rates of the above processes in strong magnetic fields to $\mathcal{O}(1/m_N)$, the first order in $1/m_N$ with m_N being the nucleon mass. Observations and theoretical considerations indicate that protoneutron stars with fields of $\sim 10^{16}$ G may be formed. The rates of the above processes in such strong fields have been studied in the literature, but the calculations were only carried out to $\mathcal{O}(1)$, the zeroth order in $1/m_N$ (see Ref. [5] and references therein). In the absence of magnetic fields, the rate of the forward process in Eq. (1b) is badly overestimated for the conditions in supernovae if the effects of nucleon recoil and weak magnetism, both of $\mathcal{O}(1/m_N)$, are ignored [6]. This suggests that calculations to $\mathcal{O}(1/m_N)$ are needed to obtain accurate rates of the processes in Eq. (1) in strong fields.

This paper is organized as follows. The energies and the wave functions of the relevant particles in magnetic fields are discussed in Sec. II. The corresponding cross sections of the neutrino absorption processes in Eq. (1) and the corresponding differential reaction rates of the reverse neutrino emission processes are derived to $\mathcal{O}(1/m_N)$ in Sec. III. The rates of these processes in supernova environments with magnetic fields of $\sim 10^{16}$ G are calculated and discussed in Sec. IV. Conclusions are given in Sec. V.

*Present address: Center for Astrophysics & Space Sciences, University of California, San Diego, La Jolla, CA 92093-0424; Electronic address: hduan@ucsd.edu

†Electronic address: qian@physics.umn.edu

II. PARTICLE ENERGIES AND WAVE FUNCTIONS IN MAGNETIC FIELDS

The importance of magnetic field effects can be gauged from the energy scale

$$\sqrt{eB} = 7.69 \left(\frac{B}{10^{16} \text{ G}} \right)^{1/2} \text{ MeV}, \quad (2)$$

where e is the charge of e^+ and B is the field strength. Observations indicate that neutron stars may have $B \sim 10^{15}$ G long after their birth in supernovae [7, 8, 9]. This suggests that at least $B \sim 10^{15}$ G can be generated during the formation of some protoneutron stars. An upper limit of $B \sim 10^{18}$ G can be estimated for such a star by equating the magnetic energy to its gravitational binding energy [10]. Here we consider that $B \sim 10^{16}$ G may exist near a protoneutron star. For such fields, the associated energy scale is much smaller than the mass of the W boson $M_W = 80$ GeV. So there will be no change in the description of the weak interaction that is involved in the processes in Eq. (1). On the other hand, the energy scale for $B \sim 10^{16}$ G is larger than the temperature ($T \sim 1$ MeV) of the material above the protoneutron star and comparable to the typical neutrino energy ($E_\nu \sim 10$ MeV). Thus, magnetic field effects on energy levels of charged particles (e^\pm and p) will be important. Furthermore, $B \sim 10^{16}$ G will induce polarization of nucleon spin at the level of $eB/m_N T \sim 10^{-2}$. This is significant due to parity violation of weak interaction and should also be taken into account.

We discuss the energy levels and the corresponding wave functions of all the relevant particles in this section. We assume a uniform magnetic field \mathbf{B} in the positive z -direction, for which the vector potential is

$$\mathbf{A} = \left(-\frac{1}{2}By, \frac{1}{2}Bx, 0 \right). \quad (3)$$

All the wave functions will be given in Dirac-Pauli representation.

A. Electron and positron

The motion of e^\pm along the z -axis is not affected by the magnetic field, but the motion in the xy -plane is quantized into Landau levels with energies (see, e.g., Ref. [11])

$$E_e = \sqrt{m_e^2 + k_{ez}^2 + 2n_e eB}, \quad (4)$$

where m_e is the rest mass of e^\pm , k_{ez} is the z -component of the momentum, and n_e is an integer quantum number (i.e., $n_e = 0, 1, 2, \dots$). For the e^\pm in the initial states of the neutrino emission processes in Eq. (1), the relevant E_e is of the order of the temperature $T \sim 1$ MeV for the material above the protoneutron star. It can be seen from Eqs. (2) and (4) that these e^\pm predominantly occupy the ground Landau level ($n_e = 0$) for $B \sim 10^{16}$ G. In comparison, the e^\pm in the final states of the neutrino absorption processes typically have E_e of the order of the neutrino energy $E_\nu \sim 10$ MeV. These e^\pm can occupy excited Landau levels ($n_e \geq 1$).

The wave function of e^- in cylindrical coordinates (ξ, ϕ, z) is

$$(\psi_{e^-})_{s_e} = \frac{e^{i(k_{ez}z - E_e t)} e^{i(n_e - r_e)\phi}}{\sqrt{2\pi L/eB}} (U_{e^-})_{s_e}, \quad (5)$$

where $s_e = 1$ and -1 for spin up and down, respectively, r_e is the quantum number labeling the center of gyromotion in the xy -plane, and L is the linear size of the normalization volume. In Eq. (5), the spinor $(U_{e^-})_{s_e}$ is

$$(U_{e^-})_{s_e=1} = \frac{1}{\sqrt{2E_e(E_e + m_e)}} \begin{pmatrix} (m_e + E_e)e^{-i\phi} I_{n_e-1, r_e}(eB\xi^2/2) \\ 0 \\ k_{ez}e^{-i\phi} I_{n_e-1, r_e}(eB\xi^2/2) \\ i\sqrt{2n_e eB} I_{n_e, r_e}(eB\xi^2/2) \end{pmatrix} \quad (6)$$

and

$$(U_{e^-})_{s_e=-1} = \frac{1}{\sqrt{2E_e(E_e + m_e)}} \begin{pmatrix} 0 \\ (m_e + E_e) I_{n_e, r_e}(eB\xi^2/2) \\ -i\sqrt{2n_e eB} e^{-i\phi} I_{n_e-1, r_e}(eB\xi^2/2) \\ -k_{ez} I_{n_e, r_e}(eB\xi^2/2) \end{pmatrix}. \quad (7)$$

The special function $I_{n,r}(\zeta)$ in the above equations is defined in Ref. [12] and can be calculated using the method given in Appendix A.

The wave function of e^+ is

$$(\psi_{e^+})_{s_e} = \frac{e^{-i(k_{ez}z - E_e t)} e^{i(n_e - r_e)\phi}}{\sqrt{2\pi L/eB}} (U_{e^+})_{s_e}, \quad (8)$$

where

$$(U_{e^+})_{s_e=1} = \frac{1}{\sqrt{2E_e(E_e + m_e)}} \begin{pmatrix} i\sqrt{2n_e eB} e^{-i\phi} I_{n_e-1, r_e}(eB\xi^2/2) \\ -k_{ez} I_{n_e, r_e}(eB\xi^2/2) \\ 0 \\ (m_e + E_e) I_{n_e, r_e}(eB\xi^2/2) \end{pmatrix} \quad (9)$$

and

$$(U_{e^+})_{s_e=-1} = \frac{1}{\sqrt{2E_e(E_e + m_e)}} \begin{pmatrix} -k_{ez} e^{-i\phi} I_{n_e-1, r_e}(eB\xi^2/2) \\ i\sqrt{2n_e eB} I_{n_e, r_e}(eB\xi^2/2) \\ -(m_e + E_e) e^{-i\phi} I_{n_e-1, r_e}(eB\xi^2/2) \\ 0 \end{pmatrix}. \quad (10)$$

Clearly, E_e does not depend on the quantum number r_e in the wave functions. This leads to a degeneracy factor

$$\sum_{r_e} 1 = \frac{eBL^2}{2\pi} \quad (11)$$

for each Landau level of e^\pm (see, e.g., Ref. [10]). Each level is further degenerate with respect to spin except for the ground level [$(\psi_{e^-})_{s_e=1} = (\psi_{e^+})_{s_e=-1} = 0$ for $n_e = 0$]. This introduces an additional spin degeneracy factor g_{n_e} , which is 1 for $n_e = 0$ and 2 for $n_e \geq 1$.

B. Proton

Protons are nonrelativistic in the supernova environment of interest. For nonrelativistic e^+ with the same charge and spin as protons, expansion of Eq. (4) to $\mathcal{O}(1/m_e)$ gives

$$E_{e, \text{NR}} = m_e + \frac{k_{ez}^2}{2m_e} + \frac{n_e eB}{m_e}. \quad (12)$$

The above equation already accounts for the contribution from the e^+ magnetic moment of $e/2m_e$. Unlike e^+ , protons have an anomalous magnetic moment of $\tilde{\mu}_p = 1.79 \mu_N$ in addition to the value $\mu_N = e/2m_p$ expected for a spin-1/2 point particle of charge e and mass m_p . Taking this into consideration, we obtain the energies of the proton Landau levels as

$$E_p = m_p + \frac{k_{pz}^2}{2m_p} + \frac{n_p eB}{m_p} - s_p \tilde{\mu}_p B, \quad (13)$$

where symbols have similar meanings to those for e^\pm . For $B \sim 10^{16}$ G, $eB/m_p \sim \tilde{\mu}_p B \sim 60$ keV. The protons in the initial states of the $\bar{\nu}_e$ absorption and ν_e emission processes in Eq. (1) have $E_p - m_p \sim T \sim 1$ MeV, and therefore, can occupy many Landau levels. By the correspondence principle, the quantum effects of the magnetic field on these protons are insignificant. However, the protons in the final states of the ν_e absorption and $\bar{\nu}_e$ emission processes are less energetic, with typical recoil energies of $E_p - m_p \sim E_\nu^2/m_p \sim 100$ keV and $\sim T^2/m_p \sim 1$ keV, respectively. Thus, proper treatment of proton Landau levels is especially important for these processes.

The proton wave function can be written as

$$(\psi_p)_{s_p} = \frac{e^{i(k_{pz}z - E_p t)} e^{i(r_p - n_p)\phi}}{\sqrt{2\pi L/eB}} (U_p)_{s_p}, \quad (14)$$

where

$$(U_p)_{s_p=1} = \begin{pmatrix} I_{n_p, r_p}(eB\xi^2/2) \\ 0 \\ -(k_{pz}/2m_p)I_{n_p, r_p}(eB\xi^2/2) \\ -ie^{i\phi}(\sqrt{2n_p eB}/2m_p)I_{n_p-1, r_p}(eB\xi^2/2) \end{pmatrix} \quad (15)$$

and

$$(U_p)_{s_p=-1} = \begin{pmatrix} 0 \\ e^{i\phi}I_{n_p-1, r_p}(eB\xi^2/2) \\ i(\sqrt{2n_p eB}/2m_p)I_{n_p, r_p}(eB\xi^2/2) \\ -e^{i\phi}(k_{pz}/2m_p)I_{n_p-1, r_p}(eB\xi^2/2) \end{pmatrix}. \quad (16)$$

Note that each proton Landau level is also degenerate with respect to the quantum number r_p , but the spin degeneracy of the excited levels is lifted due to the contribution from the anomalous magnetic moment.

The proton wave function contains terms of the form

$$\Psi_{n,r} \equiv \frac{e^{ik_z z} e^{i(r-n)\phi}}{\sqrt{2\pi L/eB}} I_{n,r}(eB\xi^2/2), \quad (17)$$

which has the following properties:

$$\pi_+ \Psi_{n-1,r} \equiv (\pi_x - i\pi_y) \Psi_{n-1,r} = i\sqrt{2neB} \Psi_{n,r}, \quad (18a)$$

and

$$\pi_- \Psi_{n,r} \equiv (\pi_x + i\pi_y) \Psi_{n,r} = -i\sqrt{2neB} \Psi_{n-1,r}. \quad (18b)$$

The operator $\boldsymbol{\pi}$ in the above equations is defined as

$$\boldsymbol{\pi} \equiv -i\boldsymbol{\nabla} - e\mathbf{A}. \quad (19)$$

Equations (18a) and (18b) can be used to simplify the evaluation of the transition amplitudes for the processes in Eq. (1) [13].

C. Neutron

Neutrons are also nonrelativistic in the supernova environment of interest, and their energy is

$$E_n = m_n + \frac{k_n^2}{2m_n} - s_n \mu_n B, \quad (20)$$

where $\mu_n = -1.91 \mu_N$ is the neutron magnetic moment. The corresponding wave function to $\mathcal{O}(1/m_N)$ is

$$(\psi_n)_{s_n} = \frac{e^{i(\mathbf{k}_n \cdot \mathbf{x} - E_n t)}}{L^{3/2}} (U_n)_{s_n}, \quad (21)$$

where

$$(U_n)_{s_n=1} = \begin{pmatrix} 1 \\ 0 \\ (k_n/2m_n) \cos \Theta_n \\ (k_n/2m_n) \sin \Theta_n e^{i\Phi_n} \end{pmatrix} \quad (22)$$

and

$$(U_n)_{s_n=-1} = \begin{pmatrix} 0 \\ 1 \\ (k_n/2m_n) \sin \Theta_n e^{-i\Phi_n} \\ -(k_n/2m_n) \cos \Theta_n \end{pmatrix}. \quad (23)$$

In the above equations, Θ_n and Φ_n are the polar and azimuthal angles of the neutron momentum \mathbf{k}_n in spherical coordinates.

D. Neutrinos

The neutrino energy is not affected by the magnetic field. For left-handed ν_e with momentum \mathbf{k}_ν , the wave function is

$$\psi_{\nu_e} = \frac{e^{i(\mathbf{k}_\nu \cdot \mathbf{x} - E_\nu t)}}{L^{3/2}} U_\nu, \quad (24)$$

where

$$U_\nu = \begin{pmatrix} \sin(\Theta_\nu/2) \\ -\cos(\Theta_\nu/2) \\ -\sin(\Theta_\nu/2) \\ \cos(\Theta_\nu/2) \end{pmatrix}. \quad (25)$$

The azimuthal angle of \mathbf{k}_ν is taken to be $\Phi_\nu = 0$ in the above equation. The wave function of right-handed $\bar{\nu}_e$ with the same momentum \mathbf{k}_ν is

$$\psi_{\bar{\nu}_e} = \frac{e^{-i(\mathbf{k}_\nu \cdot \mathbf{x} - E_\nu t)}}{L^{3/2}} U_\nu, \quad (26)$$

where U_ν is the same as in Eq. (25).

III. CROSS SECTIONS AND DIFFERENTIAL REACTION RATES

As discussed in Sec. II, $B \sim 10^{16}$ G will not affect the weak interaction, which is still described by the effective four-fermion Lagrangian

$$\mathcal{L}_{\text{int}} = \frac{G_F \cos \theta_C}{\sqrt{2}} (N_\alpha^\dagger L^\alpha + N^\alpha L_\alpha^\dagger), \quad (27)$$

where $G_F = (292.8 \text{ GeV})^{-2}$ is the Fermi constant, θ_C is the Cabibbo angle ($\cos^2 \theta_C = 0.95$), the leptonic charged current L^α is

$$L^\alpha = \bar{\psi}_\nu \gamma^\alpha (1 - \gamma_5) \psi_e, \quad (28)$$

and the nucleonic current N^α is

$$N^\alpha = \bar{\psi}_p \left[f \gamma^\alpha - g \gamma^\alpha \gamma_5 + \frac{if_2}{2m_p} \sigma^{\alpha\beta} (-i \overleftrightarrow{\mathcal{D}}_\beta) \right] \psi_n. \quad (29)$$

In the above equations, γ^α , γ_5 , and $\sigma^{\alpha\beta}$ are the standard matrices describing fermionic transitions in Dirac-Pauli representation, and $f = 1$, $g = 1.26$, and $f_2 = 3.7$ are the nucleon form factors. The term involving f_2 in Eq. (29) represents weak magnetism and must be included for calculations to $\mathcal{O}(1/m_N)$. The covariant derivative $-i \overleftrightarrow{\mathcal{D}}_\beta$ in this term preserves the gauge invariance and operates according to

$$\bar{\psi}_p O (-i \overleftrightarrow{\mathcal{D}}_\beta) \psi_n = [(-i \partial_\beta - e A_\beta) \bar{\psi}_p] O \psi_n - \bar{\psi}_p O (i \partial_\beta \psi_n), \quad (30)$$

where O is a constant matrix and A_β corresponds to the electromagnetic field ($A_0 = 0$ here). Based on the above description of the weak interaction, we derive below the cross sections of the neutrino absorption processes in Eq. (1) and the differential reaction rates of the reverse neutrino emission processes. We will include the magnetic field effects on particle energies and wave functions and focus on corrections of $\mathcal{O}(1/m_N)$ in both the transition amplitude and kinematics. Radiative corrections will be ignored.

A. Cross sections for neutrino absorption

We first derive the cross section of $\nu_e + n \rightarrow e^- + p$ in detail. The transition matrix of this process is

$$\mathcal{T}_{\nu_e n} = \frac{G_F \cos \theta_C}{\sqrt{2}} \int \bar{\psi}_p \left[f \gamma^\alpha - g \gamma^\alpha \gamma_5 + \frac{if_2}{2m_p} \sigma^{\alpha\beta} (-i \overleftrightarrow{\mathcal{D}}_\beta) \right] \psi_n \bar{\psi}_{e^-} \gamma_\alpha (1 - \gamma_5) \psi_{\nu_e} d^4x. \quad (31)$$

With the wave functions given in Sec. II, Eq. (31) can be rewritten as

$$\mathcal{T}_{\nu_e n} = \frac{G_F \cos \theta_C}{\sqrt{2}} \frac{eB}{2\pi L^4} 2\pi \delta(E_e + E_p - E_\nu - E_n) 2\pi \delta(k_{ez} + k_{pz} - k_{\nu z} - k_{nz}) \mathfrak{M}_{\nu_e n}. \quad (32)$$

The amplitude $\mathfrak{M}_{\nu_e n}$ in Eq. (32) is

$$\begin{aligned} \mathfrak{M}_{\nu_e n} = & \int_0^\infty \xi d\xi \int_0^{2\pi} e^{i\mathbf{w}_\perp \cdot \mathbf{x}_\perp} e^{-i(n_e - r_e - n_p + r_p)\phi} \left\{ \bar{U}_p \gamma^\alpha (f - g\gamma_5) U_n \bar{U}_{e-} \gamma_\alpha (1 - \gamma_5) U_{\nu_e} \right. \\ & \left. + \frac{if_2}{2m_p} \left[(X_p)_\beta^\dagger \gamma^0 \sigma^{\alpha\beta} U_n - (k_n)_\beta \bar{U}_p \sigma^{\alpha\beta} U_n \right] \bar{U}_{e-} \gamma_\alpha (1 - \gamma_5) U_{\nu_e} \right\} d\phi, \end{aligned} \quad (33)$$

where $\mathbf{w} = \mathbf{k}_n + \mathbf{k}_\nu$ is the total momentum, the subscript \perp denotes a vector in the xy -plane, and

$$(X_p)_\beta \equiv \left[\frac{e^{i(k_{pz}z - E_p t)} e^{i(r_p - n_p)\phi}}{\sqrt{2\pi L/eB}} \right]^{-1} (i\partial_\beta - eA_\beta) \psi_p. \quad (34)$$

Evaluation of $(X_p)_\beta$ for $\beta = 1$ and 2 (x and y) can be simplified by using Eqs. (18a) and (18b) [13].

The δ -functions in Eq. (32) enforce conservation of energy and of momentum in the z -direction, for which both the neutron and the proton momenta must be taken into account in calculations to $\mathcal{O}(1/m_N)$. For $\nu_e + n \rightarrow e^- + p$ occurring in the material above the protoneutron star, the neutron momentum is especially important as the typical value $k_n \sim \sqrt{2m_n T} = 43(T/\text{MeV})^{1/2}$ MeV is larger than the typical ν_e momentum $k_\nu = E_\nu \sim 10$ MeV. To account for this, we average the cross section over the normalized thermal distribution function $f_n(\mathbf{k}_n, s_n)$ for the neutrons and obtain

$$\sigma_{\nu_e n}^{(1,B)} = \sum_{s_n} \int f_n(\mathbf{k}_n, s_n) d^3 k_n \sum_{s_p, n_p, r_p} \int \frac{L dk_{pz}}{2\pi} \sum_{s_e, n_e, r_e} \int \frac{L dk_{ez}}{2\pi} \frac{1}{L^{-3} L^{-3}} \frac{|\mathcal{T}_{\nu_e n}|^2}{\tau L^3}, \quad (35)$$

where the superscript $(1, B)$ denotes the cross section to $\mathcal{O}(1/m_N)$ and in the presence of a magnetic field, τ is the duration of the interaction, and

$$f_n(\mathbf{k}_n, s_n) = \frac{e^{-(E_n - m_n)/T}}{(2\pi m_n T)^{3/2} (e^{\mu_n B/T} + e^{-\mu_n B/T})}. \quad (36)$$

The summation and integration in Eq. (35) must be treated as nested integrals. For example, the summation over s_n and the integration over \mathbf{k}_n apply to not only $f_n(\mathbf{k}_n, s_n)$ but also the subsequent terms that have implicit dependence on s_n and \mathbf{k}_n . The summation and integration in the equations below should be interpreted similarly.

Using

$$\begin{aligned} & \int \delta(E_e + E_p - E_\nu - E_n) \delta(k_{ez} + k_{pz} - k_{\nu z} - k_{nz}) d^3 k_n \\ &= \int d\Phi_n \int \delta(E_e + E_p - E_\nu - E_n) d\left(\frac{k_{n\perp}^2}{2}\right) \int \delta(k_{ez} + k_{pz} - k_{\nu z} - k_{nz}) dk_{nz} \\ &= m_n \int d\Phi_n \end{aligned} \quad (37)$$

to integrate over the neutron momentum, we can rewrite Eq. (35) as

$$\begin{aligned} \sigma_{\nu_e n}^{(1,B)} = & \frac{G_F^2 \cos^2 \theta_C}{4\pi} \frac{m_n eB}{(2\pi m_n T)^{3/2}} \frac{1}{e^{\mu_n B/T} + e^{-\mu_n B/T}} \\ & \times \sum_{n_e=0}^\infty \sum_{n_p=0}^\infty \int_{-\infty}^{+\infty} dk_{ez} \sum_{s_n=\pm 1} \sum_{s_p=\pm 1} \int_K dk_{pz} \int_0^{2\pi} e^{-(E_n - m_n)/T} \mathcal{W}_{\nu_e n} d\Phi_n, \end{aligned} \quad (38)$$

where

$$\mathcal{W}_{\nu_e n} \equiv \frac{eB}{2\pi L^2} \sum_{s_e, r_e, r_p} |\mathfrak{M}_{\nu_e n}|^2 \quad (39)$$

is the reduced amplitude squared given explicitly in Appendix B. It follows from Eq. (37) that E_n and k_{nz} in the integrand in Eq. (38) are determined in terms of other quantities by conservation of energy and of momentum in the z -direction. The integration region K of $\int dk_{pz}$ in Eq. (38) is also set by these conservation laws, which require

$$E_\nu + m_n + \frac{k_{n\perp}^2}{2m_n} + \frac{(k_{ez} + k_{pz} - k_{\nu z})^2}{2m_n} - s_n \mu_n B = \sqrt{m_e^2 + k_{ez}^2 + 2n_e e B} \\ + m_p + \frac{k_{pz}^2}{2m_p} + \frac{n_p e B}{m_p} - s_p \tilde{\mu}_p B. \quad (40)$$

The above equation can be rearranged into the form

$$a k_{pz}^2 + b k_{pz} + c = \frac{k_{n\perp}^2}{2m_n} \geq 0, \quad (41)$$

where

$$a = \frac{\Delta}{2m_p m_n}, \quad (42a)$$

$$b = \frac{k_{\nu z} - k_{ez}}{m_n}, \quad (42b)$$

$$c = \sqrt{m_e^2 + k_{ez}^2 + 2n_e e B} - E_\nu - \Delta - \frac{(k_{\nu z} - k_{ez})^2}{2m_n} + \frac{n_p e B}{m_p} - s_p \tilde{\mu}_p B + s_n \mu_n B, \quad (42c)$$

$$\Delta \equiv m_n - m_p. \quad (42d)$$

Thus,

$$K = \begin{cases} (-\infty, +\infty), & \text{if } b^2 \leq 4ac, \\ (-\infty, (k_{pz})_-] \cup [(k_{pz})_+, +\infty), & \text{if } b^2 > 4ac, \end{cases} \quad (43)$$

where

$$(k_{pz})_\pm = \frac{-b \pm \sqrt{b^2 - 4ac}}{2a}. \quad (44)$$

For $\bar{\nu}_e + p \rightarrow e^+ + n$ occurring in the material above the protoneutron star, the cross section can be written as

$$\sigma_{\bar{\nu}_e p}^{(1,B)} = \overline{\sum_{r_p}} \sum_{s_p, n_p} \int f_p(k_{pz}, n_p, s_p) dk_{pz} \sum_{s_n} \int \frac{L^3 d^3 k_n}{(2\pi)^3} \sum_{s_e, n_e, r_e} \int \frac{L dk_{ez}}{2\pi} \frac{1}{L^{-3} L^{-3}} \frac{|\mathcal{T}_{\bar{\nu}_e p}|^2}{\tau L^3}, \quad (45)$$

where

$$\overline{\sum_{r_p}} \equiv \left(\frac{e B L^2}{2\pi} \right)^{-1} \sum_{r_p} \quad (46)$$

and

$$f_p(k_{pz}, n_p, s_p) = \frac{e^{-(E_p - m_p)/T}}{\sqrt{2\pi m_p T}} \frac{1 - e^{-eB/m_p T}}{e^{\tilde{\mu}_p B/T} + e^{-(\tilde{\mu}_p B/T) - (eB/m_p T)}} \quad (47)$$

is the normalized thermal distribution function for the protons. Using again the integration over the neutron momentum to get rid of the δ -functions, we obtain

$$\sigma_{\bar{\nu}_e p}^{(1,B)} = \frac{G_F^2 \cos^2 \theta_C}{8\pi^2} \frac{m_n}{\sqrt{2\pi m_p T}} \frac{1 - e^{-eB/m_p T}}{e^{\tilde{\mu}_p B/T} + e^{-(\tilde{\mu}_p B/T) - (eB/m_p T)}} \\ \times \sum_{n_e=0}^{\infty} \sum_{n_p=0}^{\infty} \int_{-\infty}^{+\infty} dk_{ez} \sum_{s_n=\pm 1} \sum_{s_p=\pm 1} \int_{K'} dk_{pz} \int_0^{2\pi} e^{-(E_p - m_p)/T} \mathcal{W}_{\bar{\nu}_e p} d\Phi_n. \quad (48)$$

The reduced amplitude squared $\mathcal{W}_{\bar{\nu}_e p}$ in the above equation can be obtained from $\mathcal{W}_{\nu_e n}$ by making the substitution

$$\begin{aligned}(E_\nu, \mathbf{k}_\nu) &\longrightarrow (-E_\nu, -\mathbf{k}_\nu), \\ (E_e, k_{ez}) &\longrightarrow (-E_e, -k_{ez}).\end{aligned}\quad (49)$$

The integration region K' of $\int dk_{pz}$ in Eq. (48) is determined from energy and momentum conservation as in Eq. (40) but with the above substitution implemented.

For application to supernova neutrinos, it is useful to further average the cross sections in Eqs. (38) and (48) over the relevant normalized neutrino energy spectra $f_\nu(E_\nu)$ to obtain

$$\langle \sigma_{\nu N} \rangle = \int \sigma_{\nu N} f_\nu(E_\nu) dE_\nu, \quad (50)$$

where $\sigma_{\nu N}$ stands for $\sigma_{\nu_e n}^{(1,B)}$ or $\sigma_{\bar{\nu}_e p}^{(1,B)}$. A typical form of $f_\nu(E_\nu)$ adopted in the literature is

$$f_\nu(E_\nu) = \frac{1}{T_\nu^3 F_2(\eta_\nu)} \frac{E_\nu^2}{\exp[(E_\nu/T_\nu) - \eta_\nu] + 1}, \quad (51)$$

where T_ν and η_ν are constant parameters and

$$F_n(\eta_\nu) \equiv \int_0^\infty \frac{x^n}{\exp(x - \eta_\nu) + 1} dx. \quad (52)$$

For the neutrino energy spectra in Eq. (51), the average neutrino energy is

$$\langle E_\nu \rangle = \frac{F_3(\eta_\nu)}{F_2(\eta_\nu)} T_\nu. \quad (53)$$

B. Differential reaction rates for neutrino emission

As can be seen from Eqs. (38), (48), and (50), the cross sections $\langle \sigma_{\nu_e n}^{(1,B)} \rangle$ and $\langle \sigma_{\bar{\nu}_e p}^{(1,B)} \rangle$ for the neutrino absorption processes $\nu_e + n \rightarrow e^- + p$ and $\bar{\nu}_e + p \rightarrow e^+ + n$, respectively, have the same generic form

$$\int dE_\nu \sum_{n_e=0}^{\infty} \sum_{n_p=0}^{\infty} \int_{-\infty}^{+\infty} dk_{ez} \sum_{s_n=\pm 1} \sum_{s_p=\pm 1} \int_{\tilde{K}} dk_{pz} \int_0^{2\pi} \mathcal{F} d\Phi_n, \quad (54)$$

where $\tilde{K} = K$ or K' , and \mathcal{F} is the integrand involving the relevant amplitude squared and distribution functions. If we use the differential reaction rates with respect to $\cos \Theta_\nu$ to describe the neutrino emission processes $e^- + p \rightarrow \nu_e + n$ and $e^+ + n \rightarrow \bar{\nu}_e + p$, then these rates also have the generic form in Eq. (54). This follows from the symmetry between the forward and reverse processes. In particular, the transition amplitudes squared $|\mathcal{T}_{e^- p}|^2$ and $|\mathcal{T}_{e^+ n}|^2$ are identical to $|\mathcal{T}_{\nu_e n}|^2$ and $|\mathcal{T}_{\bar{\nu}_e p}|^2$, respectively. By taking advantage of the symmetry between the neutrino absorption and emission processes, numerical computation of the cross sections for the former and the differential reaction rates for the latter is greatly simplified.

For $e^- + p \rightarrow \nu_e + n$ occurring in the material above the protoneutron star, the differential reaction rate is

$$\begin{aligned}\frac{d\lambda_{e^- p}^{(1,B)}}{d \cos \Theta_\nu} &= \sum_{r_p} \sum_{s_p, n_p} \int f_p(k_{pz}, n_p, s_p) dk_{pz} \sum_{s_e, n_e, r_e} \int \frac{L dk_{ez}}{2\pi} \frac{1}{L^3} \frac{1}{e^{(E_e/T) - \eta_e} + 1} \\ &\times \int \frac{L^3 E_\nu^2 dE_\nu}{4\pi^2} \sum_{s_n} \int \frac{L^3 d^3 k_n}{(2\pi)^3} \frac{1}{L^{-3} L^{-3}} \frac{|\mathcal{T}_{\nu_e n}|^2}{\tau L^3},\end{aligned}\quad (55)$$

where η_e is the degeneracy parameter characterizing the Fermi-Dirac distribution function of the electrons. Integrating

over the neutron momentum as in Eq. (37), we obtain

$$\begin{aligned} \frac{d\lambda_{e^-p}^{(1,B)}}{d\cos\Theta_\nu} &= \frac{G_F^2 \cos^2\theta_C}{32\pi^4} \frac{m_n}{\sqrt{2\pi m_p T}} \frac{1 - e^{-eB/m_p T}}{e^{\bar{\mu}_p B T} + e^{-(\bar{\mu}_p B/T) - (eB/m_p T)}} \int_0^\infty E_\nu^2 dE_\nu \\ &\times \sum_{n_e=0}^\infty \sum_{n_p=0}^\infty \int_{-\infty}^{+\infty} dk_{ez} \sum_{s_n=\pm 1} \sum_{s_p=\pm 1} \int_K dk_{pz} \\ &\times \int_0^{2\pi} \frac{e^{-(E_p - m_p)/T}}{e^{(E_e/T) - \eta_e} + 1} \mathcal{W}_{\nu_e n} d\Phi_n. \end{aligned} \quad (56)$$

Similarly, we obtain the differential reaction rate for $e^+ + n \rightarrow \bar{\nu}_e + p$ as

$$\begin{aligned} \frac{d\lambda_{e^+n}^{(1,B)}}{d\cos\Theta_\nu} &= \sum_{s_n} \int f_n(\mathbf{k}_n, s_n) d^3 k_n \sum_{s_e, n_e, r_e} \int \frac{L dk_{ez}}{2\pi} \frac{1}{L^3} \frac{1}{e^{(E_e/T) + \eta_e} + 1} \\ &\times \int \frac{L^3 E_\nu^2 dE_\nu}{4\pi^2} \sum_{s_p, n_p, r_p} \int \frac{L dk_{pz}}{2\pi} \frac{1}{L^{-3} L^{-3}} \frac{|\mathcal{T}_{\bar{\nu}_e p}|^2}{\tau L^3} \\ &= \frac{G_F^2 \cos^2\theta_C}{16\pi^3} \frac{m_n e B}{(2\pi m_n T)^{3/2}} \frac{1}{e^{\mu_n B/T} + e^{-\mu_n B/T}} \int_0^\infty E_\nu^2 dE_\nu \\ &\times \sum_{n_e=0}^\infty \sum_{n_p=0}^\infty \int_{-\infty}^{+\infty} dk_{ez} \sum_{s_n=\pm 1} \sum_{s_p=\pm 1} \int_{K'} dk_{pz} \\ &\times \int_0^{2\pi} \frac{e^{-(E_n - m_n)/T}}{e^{(E_e/T) + \eta_e} + 1} \mathcal{W}_{\bar{\nu}_e p} d\Phi_n. \end{aligned} \quad (57)$$

IV. RATES OF NEUTRINO PROCESSES IN SUPERNOVAE

We now calculate the rates of the neutrino absorption and emission processes in Eq. (1) for the supernova environment near a protoneutron star that possesses a strong magnetic field. A wide range of heavy elements may be produced during the ejection of the material above the protoneutron star. As mentioned in the introduction, a key parameter governing this production is the neutron-to-proton ratio of the material [3, 4], which depends on the competition between the neutrino absorption and emission processes [2]. We will calculate the rates of these processes in the context of heavy element nucleosynthesis, for which the accuracy of these rates is especially important. In this context, the material above the protoneutron star is characterized by temperatures of $T \sim 1$ MeV, entropies of $S \sim 100$ (in units of Boltzmann constant per nucleon), and electron fractions of $Y_e \lesssim 0.5$. For these conditions, the nucleons in the material are nonrelativistic and nondegenerate while the e^\pm are relativistic and have a small degeneracy parameter $0 < \eta_e \ll 1$. The thermal distribution functions of the nucleons and e^\pm have been given in Sec. III. The neutrinos emitted from the protoneutron star are not in thermal equilibrium with the overlying material and their energy distribution functions are taken to be of the form in Eq. (51). As discussed in Ref. [5], Pauli blocking for the final states of the neutrino processes above the protoneutron star is unimportant and will be ignored.

A. Neutrino absorption

At a radius R above the protoneutron star, the rate of neutrino absorption per nucleon can be estimated as

$$\lambda_{\nu N} = \frac{L_\nu \langle \sigma_{\nu N} \rangle}{4\pi R^2 \langle E_\nu \rangle} = 49.7 \left(\frac{L_\nu}{10^{51} \text{ erg s}^{-1}} \right) \left(\frac{10 \text{ MeV}}{\langle E_\nu \rangle} \right) \left(\frac{\langle \sigma_{\nu N} \rangle}{10^{-41} \text{ cm}^2} \right) \left(\frac{10 \text{ km}}{R} \right)^2 \text{ s}^{-1}, \quad (58)$$

where L_ν is the neutrino luminosity and has a typical value of $\sim 10^{51}$ erg s $^{-1}$ in the supernova epoch of interest. The key quantity $\langle \sigma_{\nu N} \rangle$ in the above equation is obtained by averaging $\sigma_{\nu N}$ over the neutrino energy spectrum. We first compare various approximations for $\sigma_{\nu N}$ as functions of the neutrino energy E_ν .

The cross sections for neutrino absorption on nucleons in a magnetic field have been derived to $\mathcal{O}(1/m_N)$ as $\sigma_{\nu N}^{(1,B)}$ in Sec. III A. To $\mathcal{O}(1)$, the zeroth order in $1/m_N$, the cross sections are [5]

$$\begin{aligned}\sigma_{\nu N}^{(0,B)} &= \sigma_{B,1} \left[1 + 2\chi \frac{(f \pm g)g}{f^2 + 3g^2} \cos \Theta_\nu \right] \\ &+ \sigma_{B,2} \left[\frac{f^2 - g^2}{f^2 + 3g^2} \cos \Theta_\nu + 2\chi \frac{(f \mp g)}{f^2 + 3g^2} \right],\end{aligned}\quad (59)$$

where

$$\sigma_{B,1} = \frac{G_F^2 \cos^2 \theta_C}{2\pi} (f^2 + 3g^2) eB \sum_{n_e=0}^{n_{e,\max}} \frac{g_{n_e} E_e^{(0)}}{\sqrt{(E_e^{(0)})^2 - m_e^2 - 2n_e eB}}, \quad (60)$$

$$\sigma_{B,2} = \frac{G_F^2 \cos^2 \theta_C}{2\pi} (f^2 + 3g^2) eB \frac{E_e^{(0)}}{\sqrt{(E_e^{(0)})^2 - m_e^2}}, \quad (61)$$

$$E_e^{(0)} = E_\nu \pm \Delta, \quad (62)$$

$$n_{e,\max} = \left[\frac{(E_e^{(0)})^2 - m_e^2}{2eB} \right]_{\text{int}}. \quad (63)$$

In the above equations and elsewhere in this subsection, the upper sign is for $\nu_e + n \rightarrow e^- + p$ and the lower sign is for $\bar{\nu}_e + p \rightarrow e^+ + n$. In Eq. (59),

$$\chi = \frac{\exp(\mu B/T) - \exp(-\mu B/T)}{\exp(\mu B/T) + \exp(-\mu B/T)} \quad (64)$$

is the polarization of nucleon spin, where μ is the magnetic moment of the relevant nucleon with $\mu_p = 2.79\mu_N$ and $\mu_n = -1.91\mu_N$. For the case of interest here, $|\mu|B/T \ll 1$, so

$$\chi = \frac{\mu B}{T} = 3.15 \times 10^{-2} \left(\frac{\mu}{\mu_N} \right) \left(\frac{B}{10^{16} \text{ G}} \right) \left(\frac{\text{MeV}}{T} \right). \quad (65)$$

For numerical examples of the cross sections, we take $B = 10^{16}$ G. The cross sections $\sigma_{\nu_e n}^{(0,B)}$ for $\cos \Theta_\nu = -1, 0, 1$ as functions of E_ν are shown as the dotted curves in Figs. 1a, 1b, and 1c, respectively. The angle-dependent terms in Eq. (59) for $\sigma_{\nu_e p}^{(0,B)}$ are proportional to the difference between f and g . As the numerical values of f and g are close, these terms are very small. So we only show the cross section $\sigma_{\bar{\nu}_e p}^{(0,B)}$ for $\cos \Theta_\nu = 0$ as the dotted curve in Fig. 1d. All the dotted curves in Fig. 1 have spikes superposed on a general trend. The varying heights of these spikes are artifacts of the plotting tool: all the spikes should have been infinitely high as they correspond to “resonances” at $E_e^{(0)} = \sqrt{m_e^2 + 2n_e eB}$, for which a new Landau level opens up. Similar to the Doppler broadening of the photon absorption lines in the solar light spectrum, these formal infinities will be smoothed out by the thermal motion of the absorbing nucleons. Such motion is of $\mathcal{O}(1/m_N)$ and has been taken into account by the cross sections $\sigma_{\nu N}^{(1,B)}$ derived in Sec. III A. Using $T = 2$ MeV for illustration, we show $\sigma_{\nu N}^{(1,B)}$ as the solid curves in Fig. 1. It can be seen that where spikes occur in $\sigma_{\nu N}^{(0,B)}$, there are only smooth bumps in $\sigma_{\nu N}^{(1,B)}$. Clearly, $\sigma_{\nu N}^{(1,B)}$ is more physical than $\sigma_{\nu N}^{(0,B)}$.

Two more aspects of Fig. 1 require discussion. First, the bumps in $\sigma_{\nu N}^{(1,B)}$ diminish as E_ν increases and become invisible for $E_\nu \gg \sqrt{eB} \sim 8$ MeV. This is expected from the correspondence principle: when a number of Landau levels for e^\pm and protons can be occupied, the quantum effects of the magnetic field are small. As noted in Sec. II B, the absorbing proton in $\bar{\nu}_e + p \rightarrow e^+ + n$ can occupy many levels for $T \sim 1$ MeV. However, for the e^+ in $\bar{\nu}_e + p \rightarrow e^+ + n$ and the e^- and the proton in $\nu_e + n \rightarrow e^- + p$, occupation of many levels requires $E_\nu \gg \sqrt{eB} \sim 8$ MeV (see Secs. II A and II B). Second, while the general trends of the dotted curves for $\sigma_{\nu_e n}^{(0,B)}$ appear to follow the corresponding solid curves for $\sigma_{\nu_e n}^{(1,B)}$, the general trend of the dotted curve for $\sigma_{\bar{\nu}_e p}^{(0,B)}$ deviates substantially from the corresponding solid curve for $\sigma_{\bar{\nu}_e p}^{(1,B)}$. This concerns the effects of weak magnetism and recoil of the final-state nucleons, both of which are of $\mathcal{O}(1/m_N)$ and are taken into account by $\sigma_{\nu N}^{(1,B)}$ but not by $\sigma_{\nu N}^{(0,B)}$. Figure 1 shows that these effects give small corrections to $\sigma_{\nu_e n}^{(0,B)}$ but much larger corrections to $\sigma_{\bar{\nu}_e p}^{(0,B)}$.

To better understand the effects of weak magnetism and recoil of the final-state nucleons, we make use of the correspondence principle. As noted above, the effects of Landau levels become negligible for $E_\nu \gg \sqrt{eB} \sim 8$ MeV.

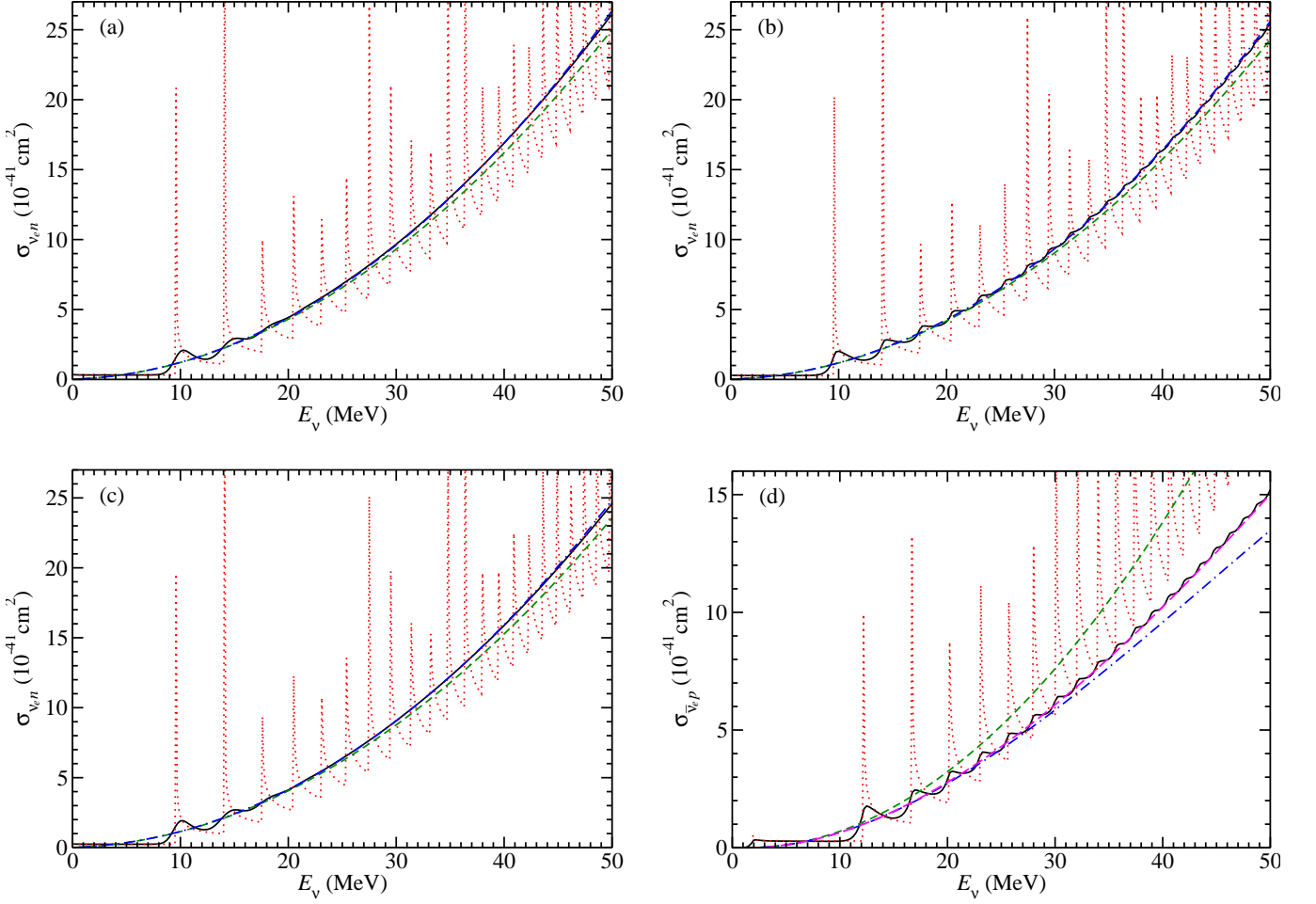


FIG. 1: (Color online) Comparison of various approximations for $\sigma_{\nu N}$ [solid curves: $\sigma_{\nu N}^{(1,B)}$; dotted curves: $\sigma_{\nu N}^{(0,B)}$; short-dashed curves: $\sigma_{\nu N}^{(0)}(1+\epsilon_\chi)$; dot-dashed curves: $\sigma_{\nu N}^{(1)}(1+\epsilon_\chi)$; long-dashed curves: $\sigma_{\nu N}^{(1*)}(1+\epsilon_\chi)$]. The dot-dashed and long-dashed curves for $\sigma_{\nu e n}$ are indistinguishable. The results for $\sigma_{\nu e n}$ are shown in (a)–(c) for $\cos \Theta_\nu = -1, 0$, and 1, respectively, while those for $\sigma_{\bar{\nu} e p}$ are shown in (d) for $\cos \Theta_\nu = 0$ ($\sigma_{\bar{\nu} e p}$ has little angular dependence). These results are calculated using $B = 10^{16}$ G, $T = 2$ MeV, $\chi_n = -0.03$, and $\chi_p = 0.04$.

In this case, the only surviving quantum effect of the magnetic field is polarization of the initial nucleon spin, which gives rise to a dependence on $\cos \Theta_\nu$ for the cross sections due to parity violation of weak interaction. Thus, allowing for this surviving effect, we should recover the results for no magnetic field in the limit of high E_ν . In the absence of any field, the cross sections $\sigma_{\nu N}^{(0)}$ and $\sigma_{\nu N}^{(1)}$ to $\mathcal{O}(1)$ and $\mathcal{O}(1/m_N)$, respectively, are (see, e.g., Refs. [6, 14])

$$\sigma_{\nu N}^{(0)} = \frac{G_F^2 \cos^2 \theta_C}{\pi} \left(E_e^{(0)} \right)^2, \quad (66)$$

$$\sigma_{\nu N}^{(1)} = \sigma_{\nu N}^{(0)} \left\{ 1 - \frac{2[f^2 + 2(f + f_2)g + 5g^2]}{f^2 + 3g^2} \frac{E_\nu}{m_N} \right\}, \quad (67)$$

where we have ignored terms like m_e^2/E_ν^2 in both equations and terms like Δ/m_N for $\sigma_{\nu N}^{(1)}$. The above zero-field cross sections assume that the initial nucleon spin is unpolarized, and therefore, do not depend on $\cos \Theta_\nu$. If a small polarization χ is artificially imposed, the modified cross sections have an additional factor $1 + \epsilon_\chi$, where

$$\epsilon_\chi = \chi \frac{2(f \pm g)g}{f^2 + 3g^2} \cos \Theta_\nu. \quad (68)$$

The term proportional to E_ν/m_N in Eq. (67) represents the effects of weak magnetism and recoil of the final-state nucleons. The coefficient in this term is 1.01 for $\nu_e + n \rightarrow e^- + p$ and -7.21 for $\bar{\nu}_e + p \rightarrow e^+ + n$. Therefore, over

TABLE I: Comparison of various approximations for $\langle \sigma_{\nu N} \rangle$ (in units of 10^{-41} cm^{-2}). These results are calculated using $\langle E_{\nu_e} \rangle = 11 \text{ MeV}$, $\langle E_{\bar{\nu}_e} \rangle = 16 \text{ MeV}$, $B = 10^{16} \text{ G}$, $T = 2 \text{ MeV}$, $\chi_n = -0.03$, and $\chi_p = 0.04$.

$\cos \Theta_\nu$	$\nu_e + n \rightarrow e^- + p$			$\bar{\nu}_e + p \rightarrow e^+ + n$		
	-1	0	1	-1	0	1
$\langle \sigma_{\nu N}^{(0)} \rangle (1 + \epsilon_\chi)$	1.67	1.62	1.57	2.49	2.48	2.46
$\langle \sigma_{\nu N}^{(1)} \rangle (1 + \epsilon_\chi)$	1.70	1.65	1.60	2.06	2.04	2.02
$\langle \sigma_{\nu N}^{(1*)} \rangle (1 + \epsilon_\chi)$	1.69	1.65	1.60	2.11	2.09	2.07
$\langle \sigma_{\nu N}^{(0,B)} \rangle$	1.65	1.57	1.50	2.50	2.46	2.42
$\langle \sigma_{\nu N}^{(1,B)} \rangle$	1.68	1.61	1.54	2.11	2.09	2.07

the range $E_\nu \sim 10\text{--}50 \text{ MeV}$ typical of supernova neutrinos, the correction due to the above effects is $\sim 1\text{--}5\%$ for the former reaction but amounts to $\sim -7\%$ to -36% for the latter reaction. The importance of these corrections has been discussed in other contexts [14, 15].

Using $\chi_n = -0.03$ and $\chi_p = 0.04$ corresponding to $B = 10^{16} \text{ G}$ and $T = 2 \text{ MeV}$, we show $\sigma_{\nu N}^{(0)}(1 + \epsilon_\chi)$ and $\sigma_{\nu N}^{(1)}(1 + \epsilon_\chi)$ as the short-dashed and dot-dashed curves, respectively, in Fig. 1. The small increase from $\sigma_{\nu_e n}^{(0)}$ to $\sigma_{\nu_e n}^{(1)}$ and the much larger decrease from $\sigma_{\bar{\nu}_e p}^{(0)}$ to $\sigma_{\bar{\nu}_e p}^{(1)}$ given in Eq. (67) can be seen from this figure. In addition, as expected from the correspondence principle, the general trends of the dotted curves for $\sigma_{\nu_e n}^{(0,B)}$ closely follow the short-dashed curves for $\sigma_{\nu_e n}^{(0)}(1 + \epsilon_{\chi_n})$ at $E_\nu \gtrsim 20 \text{ MeV}$ and the solid curves for $\sigma_{\nu_e n}^{(1,B)}$ become indistinguishable from the dot-dashed curves for $\sigma_{\nu_e n}^{(1)}(1 + \epsilon_{\chi_n})$ in the same regime (see Figs. 1a–c). However, while the relation between the dotted curve for $\sigma_{\nu_e n}^{(0,B)}$ and the short-dashed curve for $\sigma_{\bar{\nu}_e p}^{(0)}(1 + \epsilon_{\chi_p})$ is in accordance with the correspondence principle, the solid curve for $\sigma_{\bar{\nu}_e p}^{(1,B)}$ clearly stays above the dot-dashed curve for $\sigma_{\bar{\nu}_e p}^{(1)}(1 + \epsilon_{\chi_p})$ at $E_\nu \gtrsim 25 \text{ MeV}$ (see Fig. 1d). This apparent violation of the correspondence principle for $\sigma_{\bar{\nu}_e p}^{(1,B)}$ and $\sigma_{\bar{\nu}_e p}^{(1)}(1 + \epsilon_{\chi_p})$ is caused by the slightly different treatments of the reaction kinematics in calculating $\sigma_{\bar{\nu}_e p}^{(1,B)}$ and $\sigma_{\bar{\nu}_e p}^{(1)}$.

We have used the transition amplitudes to $\mathcal{O}(1/m_N)$ in calculating both $\sigma_{\nu N}^{(1,B)}$ and $\sigma_{\nu N}^{(1)}$. However, we have treated the reaction kinematics exactly for $\sigma_{\nu N}^{(1,B)}$ [assuming nonrelativistic nucleons, see Eqs. (40–44)] but only to $\mathcal{O}(1/m_N)$ for $\sigma_{\nu N}^{(1)}$. This difference does not affect the comparison between $\sigma_{\nu_e n}^{(1,B)}$ and $\sigma_{\nu_e n}^{(1)}(1 + \epsilon_{\chi_n})$ as the total correction from weak magnetism and nucleon recoil is small to $\mathcal{O}(1/m_N)$ in this case, and the terms of orders higher than $\mathcal{O}(1/m_N)$ are even smaller. In contrast, the importance of the weak magnetism and recoil effects for $\bar{\nu}_e + p \rightarrow e^+ + n$ enables terms of orders higher than $\mathcal{O}(1/m_N)$ to give rather large corrections to the cross section. Such terms are included in $\sigma_{\bar{\nu}_e p}^{(1,B)}$ due to exact treatment of the reaction kinematics but not in $\sigma_{\bar{\nu}_e p}^{(1)}$. In Ref. [16], the zero-field cross sections for neutrino absorption on nucleons were derived to $\mathcal{O}(1/m_N)$ but with reaction kinematics treated exactly. We denote these cross sections as $\sigma_{\nu N}^{(1*)}$. For consistency with the rest of the paper, we ignore radiative corrections and the effect of the Coulomb interaction between the final-state particles for $\nu_e + n \rightarrow e^- + p$, both of which were taken into account in Ref. [16]. It was shown in this reference that $\sigma_{\bar{\nu}_e p}^{(1*)}$ is more accurate than $\sigma_{\bar{\nu}_e p}^{(1)}$. We show $\sigma_{\nu N}^{(1*)}(1 + \epsilon_\chi)$ as the long-dashed curves in Fig. 1. It can be seen that the long-dashed curves for $\sigma_{\nu_e n}^{(1*)}(1 + \epsilon_{\chi_n})$ are indistinguishable from the corresponding dot-dashed curves for $\sigma_{\nu_e n}^{(1)}(1 + \epsilon_{\chi_n})$ over the range of E_ν shown but the long-dashed curve for $\sigma_{\bar{\nu}_e p}^{(1*)}(1 + \epsilon_{\chi_p})$ lies significantly above the dot-dashed curve for $\sigma_{\bar{\nu}_e p}^{(1)}(1 + \epsilon_{\chi_p})$ at $E_\nu \gtrsim 25 \text{ MeV}$. In addition, the solid curves for $\sigma_{\nu_e n}^{(1,B)}$ and $\sigma_{\bar{\nu}_e p}^{(1,B)}$ settle down to the corresponding long-dashed curves for $\sigma_{\nu_e n}^{(1*)}(1 + \epsilon_{\chi_n})$ and $\sigma_{\bar{\nu}_e p}^{(1*)}(1 + \epsilon_{\chi_p})$ at $E_\nu \gtrsim 20$ and 25 MeV , respectively. Thus, the cross sections $\sigma_{\nu_e n}^{(1,B)}$ and $\sigma_{\bar{\nu}_e p}^{(1,B)}$ calculated above are in full agreement with the correspondence principle.

We now calculate the average cross sections $\langle \sigma_{\nu N} \rangle$ using the neutrino energy spectra in Eq. (51). We take $\eta_{\nu_e} = \eta_{\bar{\nu}_e} = 3$, $\langle E_{\nu_e} \rangle = 11 \text{ MeV}$, and $\langle E_{\bar{\nu}_e} \rangle = 16 \text{ MeV}$. For these parameters, $T_{\nu_e} = 2.75 \text{ MeV}$ and $T_{\bar{\nu}_e} = 4 \text{ MeV}$. Adopting the same B , T , χ_n , and χ_p as for Fig. 1, we give $\langle \sigma_{\nu N}^{(0)} \rangle (1 + \epsilon_\chi)$, $\langle \sigma_{\nu N}^{(1)} \rangle (1 + \epsilon_\chi)$, $\langle \sigma_{\nu N}^{(1*)} \rangle (1 + \epsilon_\chi)$, $\langle \sigma_{\nu N}^{(0,B)} \rangle$, and $\langle \sigma_{\nu N}^{(1,B)} \rangle$ for $\cos \Theta_\nu = -1$, 0 , and 1 , respectively, in Table I. As discussed above, $\sigma_{\nu N}^{(1)}$ and $\sigma_{\nu N}^{(1*)}$ differ from $\sigma_{\nu N}^{(0)}$ due to the effects of weak magnetism and recoil of the final-state nucleons. These effects slightly increase the cross sections for $\nu_e + n \rightarrow e^- + p$ but substantially decrease those for $\bar{\nu}_e + p \rightarrow e^+ + n$. As can be seen from Table I, $\langle \sigma_{\nu_e n}^{(1)} \rangle (1 + \epsilon_{\chi_n})$ and $\langle \sigma_{\nu_e n}^{(1*)} \rangle (1 + \epsilon_{\chi_n})$ are only a few percent larger than $\langle \sigma_{\nu_e n}^{(0)} \rangle (1 + \epsilon_{\chi_n})$ but $\langle \sigma_{\bar{\nu}_e p}^{(1)} \rangle (1 + \epsilon_{\chi_p})$ and $\langle \sigma_{\bar{\nu}_e p}^{(1*)} \rangle (1 + \epsilon_{\chi_p})$ are $\sim 20\%$ smaller than $\langle \sigma_{\bar{\nu}_e p}^{(0)} \rangle (1 + \epsilon_{\chi_p})$. The differences between $\langle \sigma_{\nu N}^{(1,B)} \rangle$ and $\langle \sigma_{\nu N}^{(0,B)} \rangle$ are similar. On the other hand, the effects of the magnetic field on the average cross sections are small for both $\nu_e + n \rightarrow e^- + p$ and $\bar{\nu}_e + p \rightarrow e^+ + n$.

For $B = 10^{16}$ G assumed above, $\langle \sigma_{\nu_e n}^{(1,B)} \rangle$ is at most 4% smaller than $\langle \sigma_{\nu_e n}^{(1)} \rangle (1 + \epsilon_{\chi_n})$ or $\langle \sigma_{\nu_e n}^{(1*)} \rangle (1 + \epsilon_{\chi_n})$ while $\langle \sigma_{\bar{\nu}_e p}^{(1,B)} \rangle$ is indistinguishable from $\langle \sigma_{\bar{\nu}_e p}^{(1*)} \rangle (1 + \epsilon_{\chi_p})$. This is because with $\langle E_{\nu_e} \rangle = 11$ MeV and $\langle E_{\bar{\nu}_e} \rangle = 16$ MeV, the important energy range for determining the average cross sections has $E_{\nu} > \sqrt{eB} \sim 8$ MeV, for which the effects of Landau levels are small. As $\langle E_{\bar{\nu}_e} \rangle$ is substantially larger than $\langle E_{\nu_e} \rangle$, the magnetic field affects $\langle \sigma_{\bar{\nu}_e p}^{(1,B)} \rangle$ even less than $\langle \sigma_{\nu_e n}^{(1,B)} \rangle$.

The results for absorption of supernova neutrinos on nucleons can be summarized as follows. Generally speaking, one can use $\langle \sigma_{\nu N}^{(1)} \rangle - \langle \sigma_{\nu N}^{(0)} \rangle$ to estimate the corrections without magnetic fields, and use $\langle \sigma_{\nu N}^{(0,B)} \rangle - \langle \sigma_{\nu N}^{(0)} \rangle$ to estimate the corrections due to magnetic fields. For $B \lesssim 10^{16}$ G, $\langle \sigma_{\nu_e n}^{(1)} \rangle + [\langle \sigma_{\nu_e n}^{(0,B)} \rangle - \langle \sigma_{\nu_e n}^{(0)} \rangle]$ is a good estimate of $\langle \sigma_{\nu_e n}^{(1,B)} \rangle$ with an accuracy of $\sim 1\%$. For the same field strength, the effects of magnetic fields are not important for $\langle \sigma_{\bar{\nu}_e p}^{(1)} \rangle$, and $\langle \sigma_{\bar{\nu}_e p}^{(1*)} \rangle$ is a good estimate of $\langle \sigma_{\bar{\nu}_e p}^{(1,B)} \rangle$ with an accuracy of $\sim 1\%$.

B. Neutrino emission

The differential reaction rates with respect to $\cos \Theta_{\nu}$ for $e^- + p \rightarrow \nu_e + n$ and $e^+ + n \rightarrow \bar{\nu}_e + p$ in a magnetic field have been derived to $\mathcal{O}(1/m_N)$ as $d\lambda_{e^- p}^{(1,B)}/d\cos \Theta_{\nu}$ and $d\lambda_{e^+ n}^{(1,B)}/d\cos \Theta_{\nu}$, respectively, in Sec. III B. To $\mathcal{O}(1)$, the zeroth order in $1/m_N$, the differential reaction rates are [5]

$$\frac{d\lambda_{eN}^{(0,B)}}{d\cos \Theta_{\nu}} = \frac{eB}{2\pi^2} \sum_{n_e} g_{n_e} \int_0^\infty \frac{d\Gamma_{eN}^{(0,B)}/d\cos \Theta_{\nu}}{\exp[(E_e/T) \mp \eta_e] + 1} dk_{ez}, \quad (69)$$

where

$$\begin{aligned} \frac{d\Gamma_{eN}^{(0,B)}}{d\cos \Theta_{\nu}} &= \frac{\Gamma_{eN}^{(0)}}{2} \left[1 + 2\chi \frac{(f \mp g)g}{f^2 + 3g^2} \cos \Theta_{\nu} \right] \\ &\quad + \delta_{n_e,0} \frac{\Gamma_{eN}^{(0)}}{2} \left[\frac{f^2 - g^2}{f^2 + 3g^2} \cos \Theta_{\nu} + 2\chi \frac{(f \pm g)g}{f^2 + 3g^2} \right], \end{aligned} \quad (70)$$

$$\Gamma_{eN}^{(0)} = \frac{G_F^2 \cos^2 \theta_C}{2\pi} (f^2 + 3g^2) (E_e \mp \Delta)^2. \quad (71)$$

In the above equations and elsewhere in this subsection, the upper sign is for $e^- + p \rightarrow \nu_e + n$ and the lower sign is for $e^+ + n \rightarrow \bar{\nu}_e + p$. In Eq. (70), $\delta_{n_e,0}$ is the Kronecker delta. For comparison, in the absence of any magnetic field, the differential reaction rates to $\mathcal{O}(1)$ are

$$\frac{d\lambda_{eN}^{(0)}}{d\cos \Theta_{\nu}} = \int \frac{\Gamma_{eN}^{(0)}}{\exp[(E_e/T) \mp \eta_e] + 1} \frac{d^3 k_e}{(2\pi)^3}. \quad (72)$$

We have also calculated $d\lambda_{eN}^{(1*)}/d\cos \Theta_{\nu}$ to $\mathcal{O}(1/m_N)$ using the prescription in Ref. [16]. Note that both $d\lambda_{eN}^{(0)}/d\cos \Theta_{\nu}$ and $d\lambda_{eN}^{(1*)}/d\cos \Theta_{\nu}$ are independent of $\cos \Theta_{\nu}$.

To compare $d\lambda_{eN}^{(1,B)}/d\cos \Theta_{\nu}$ with $d\lambda_{eN}^{(0,B)}/d\cos \Theta_{\nu}$, we take $B = 10^{16}$ G, $T = 2$ MeV, and $\eta_e = 0$. The differential reaction rates $d\lambda_{eN}^{(1,B)}/d\cos \Theta_{\nu}$ are numerically calculated for $\Theta_{\nu} = 0, \pi/4, \pi/2, 3\pi/4$, and π and shown as the filled circles with error bars in Fig. 2. Here and elsewhere in this subsection, the error bars for our results represent the accuracy of the numerical calculation. To very good approximation, the rates $d\lambda_{eN}^{(1,B)}/d\cos \Theta_{\nu}$ are linear functions of $\cos \Theta_{\nu}$ as shown by the solid lines fitted to the numerical results in Fig. 2. The rates $d\lambda_{eN}^{(0,B)}/d\cos \Theta_{\nu}$ as functions of $\cos \Theta_{\nu}$ are shown as the dashed lines in the same figure. It can be seen that relative to $d\lambda_{e^- p}^{(0,B)}/d\cos \Theta_{\nu}$, $d\lambda_{e^- p}^{(1,B)}/d\cos \Theta_{\nu}$ is smaller for $\cos \Theta_{\nu} \gtrsim 0.15$ but larger for $\cos \Theta_{\nu} < 0.15$ due to corrections of $\mathcal{O}(1/m_N)$. So we expect that when integrated over $\cos \Theta_{\nu}$, the difference between $\lambda_{e^- p}^{(0,B)}$ and $\lambda_{e^- p}^{(1,B)}$ is small. In contrast, corrections of $\mathcal{O}(1/m_N)$ make $d\lambda_{e^+ n}^{(1,B)}/d\cos \Theta_{\nu}$ smaller than $d\lambda_{e^+ n}^{(0,B)}/d\cos \Theta_{\nu}$ for all values of $\cos \Theta_{\nu}$. As discussed in the case of neutrino absorption, such corrections are due to the effects of weak magnetism and recoil of the final-state nucleons, which tend to affect the processes involving $\bar{\nu}_e$ more than those involving ν_e . These corrections can also be seen by comparing the zero-field results $d\lambda_{eN}^{(0)}/d\cos \Theta_{\nu}$ and $d\lambda_{eN}^{(1*)}/d\cos \Theta_{\nu}$, which are shown as the dotted and dot-dashed lines, respectively, in Fig. 2. Note that for the parameters adopted above, the magnetic field decreases the rates for $e^- + p \rightarrow \nu_e + n$ but increases those for $e^+ + n \rightarrow \bar{\nu}_e + p$.

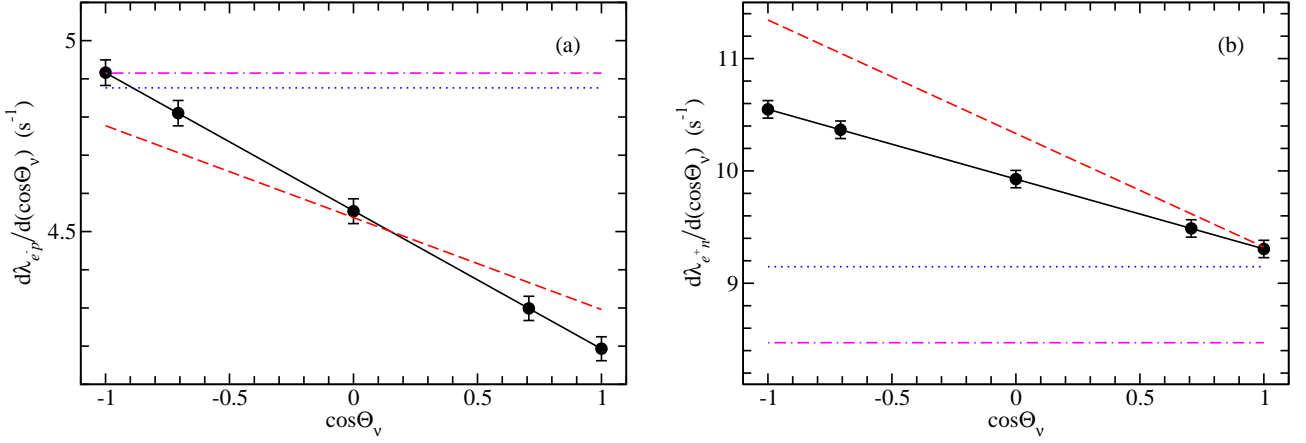


FIG. 2: (Color online) Comparison of various approximations for $d\lambda_{eN}/d \cos \Theta_\nu$ [filled circles with error bars: $d\lambda_{eN}^{(1,B)}/d \cos \Theta_\nu$; dashed lines: $d\lambda_{eN}^{(0,B)}/d \cos \Theta_\nu$; dotted lines: $d\lambda_{eN}^{(0)}/d \cos \Theta_\nu = \lambda_{eN}^{(0)}/2$; dot-dashed lines: $d\lambda_{eN}^{(1*)}/d \cos \Theta_\nu = \lambda_{eN}^{(1*)}/2$]. The error bars on the filled circles represent the accuracy of the numerical calculation and the solid lines are linear fits to the filled circles. These results are calculated using $B = 10^{16}$ G, $T = 2$ MeV, and $\eta_e = 0$.

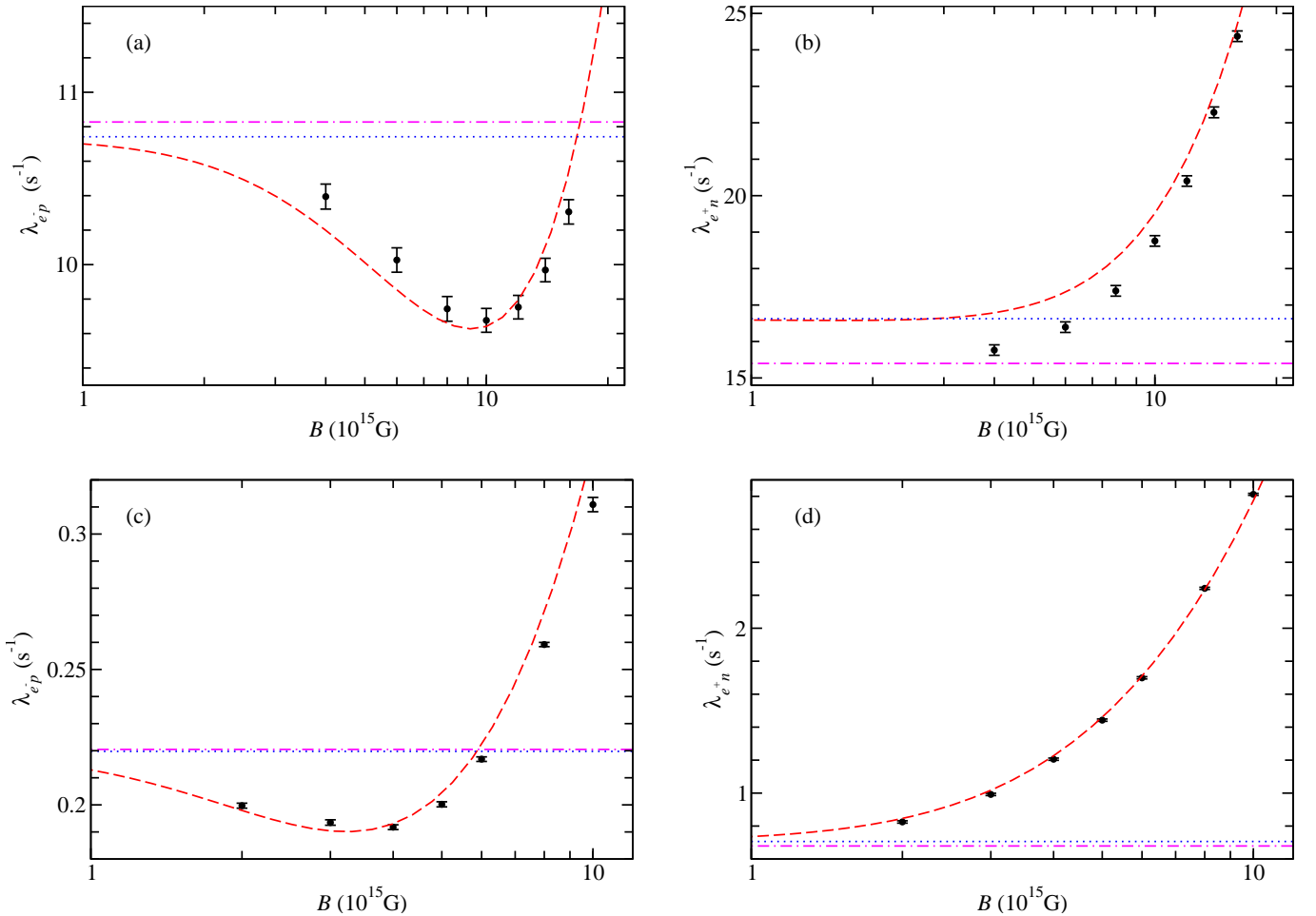


FIG. 3: (Color online) Comparison of various approximations for λ_{eN} [filled circles with error bars: $\lambda_{eN}^{(1,B)}$; dashed curves: $\lambda_{eN}^{(0,B)}$; dotted lines: $\lambda_{eN}^{(0)}$; dot-dashed lines: $\lambda_{eN}^{(1*)}$]. These results are calculated using two sets of conditions: $(T, S, Y_e) = (2 \text{ MeV}, 50, 0.5)$ for (a) and (b) and $(1 \text{ MeV}, 100, 0.5)$ for (c) and (d). The error bars on the filled circles represent the accuracy of the numerical calculation.

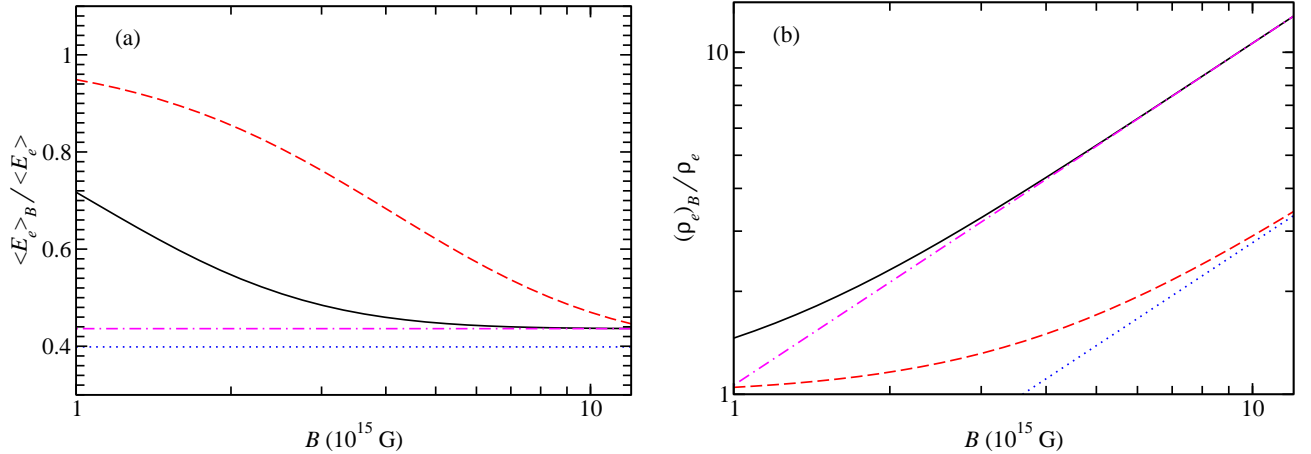


FIG. 4: (Color online) The ratios $\langle E_e \rangle_B / \langle E_e \rangle$ (a) and $(\rho_e)_B / \rho_e$ (b) as functions of B (solid curves: $T = 1$ MeV; dashed curves: $T = 2$ MeV). The limiting case where all e^\pm are in the ground Landau level is shown as the dot-dashed ($T = 1$ MeV) and dotted ($T = 2$ MeV) lines. These results are calculated using $\eta_e = 0$ for simplicity.

To further explore the effects of the magnetic field on the rates of neutrino emission, we consider two representative sets of supernova conditions: $(T, S, Y_e) = (2$ MeV, 50, 0.5) and $(1$ MeV, 100, 0.5) for cases I and II, respectively. For each case, the electron degeneracy parameter η_e can be obtained from the equations of state as discussed in Ref. [5]. We calculate the rates $\lambda_{eN}^{(1,B)}$ for a number of values of B (4×10^{15} – 1.6×10^{16} G for case I and 2×10^{15} – 10^{16} G for case II) and show the results as the filled circles with error bars in Fig. 3. The corresponding rates $\lambda_{eN}^{(0,B)}$ as functions of B and the zero-field results $\lambda_{eN}^{(0)}$ and $\lambda_{eN}^{(1*)}$ are shown as the dashed curves and dotted and dot-dashed lines, respectively, in the same figure. As can be seen from Fig. 3, in the limit of small B , the dashed curves for $\lambda_{eN}^{(0,B)}$ agree with the dotted curves for $\lambda_{eN}^{(0)}$. The approach of $\lambda_{e+n}^{(1,B)}$ (filled circles) to the zero-field limit $\lambda_{e+n}^{(1*)}$ (dot-dashed line) is also clearly demonstrated for case I. As a large number of Landau levels must be included in the calculation for small B , it becomes computationally prohibitive to demonstrate the behavior of $\lambda_{eN}^{(1,B)}$ in this limit to the fullest extent. Nevertheless, the relation between $\lambda_{eN}^{(1,B)}$ and $\lambda_{eN}^{(0,B)}$ for small B clearly agrees with that between $\lambda_{eN}^{(1*)}$ and $\lambda_{eN}^{(0)}$.

The dependences on B for the rates of neutrino emission shown in Fig. 3 require discussion. The effects of the magnetic field on these rates have been noted for the specific case of $B = 10^{16}$ G, $T = 2$ MeV, and $\eta_e = 0$ shown in Fig. 2. More generally, Fig. 3 shows that $\lambda_{e-p}^{(0,B)}$ and $\lambda_{e-p}^{(1,B)}$ first decrease with increasing B to reach some minimum values and then increase with B . In contrast, $\lambda_{e+n}^{(0,B)}$ and $\lambda_{e+n}^{(1,B)}$ monotonically increase with B . The above results can be understood by considering two different effects of the magnetic field on e^\pm . On the one hand, a stronger field confines more e^\pm to the ground Landau level, thus reducing the average e^\pm energy. This tends to decrease the rates of neutrino emission. On the other hand, a magnetic field changes the e^\pm phase space according to

$$2 \int \frac{d^3 k_e}{(2\pi)^3} \rightarrow \frac{eB}{4\pi^2} \sum_{n_e} g_{n_e} \int_{-\infty}^{+\infty} dk_{ez}. \quad (73)$$

Thus, the e^\pm phase space increases with B , which tends to increase the rates of neutrino emission due to the increase in the number density of e^\pm . The competition between the above two factors then determines the dependences on B for the rates of neutrino emission.

To show quantitatively the two effects of the magnetic field on e^\pm discussed above, we compare the average energy $\langle E_e \rangle_B$ and the number density $(\rho_e)_B$ of e^\pm in a field with the corresponding quantities for no field, $\langle E_e \rangle$ and ρ_e , respectively, for a wide range of B in Fig. 4. As $0 < \eta_e \ll 1$ for the supernova conditions represented by cases I and II, we take $\eta_e = 0$ for simplicity. The major difference between these two cases lies in the temperature. The ratios $\langle E_e \rangle_B / \langle E_e \rangle$ as functions of B for $T = 1$ and 2 MeV (cases II and I) are shown as the solid and dashed curves, respectively, in Fig. 4a. The corresponding ratios $(\rho_e)_B / \rho_e$ are shown in Fig. 4b. For large B , it is appropriate to consider the limiting case where all e^\pm are in the ground Landau level, and therefore, $\langle E_e \rangle_B / \langle E_e \rangle$ is a constant and $(\rho_e)_B / \rho_e$ increases linearly with B . These limits are shown as the dot-dashed and dotted lines for $T = 1$ and 2

MeV, respectively, in Fig. 4. As can be seen from this figure, $\langle E_e \rangle_B / \langle E_e \rangle$ monotonically decreases with increasing B , eventually approaching the constant limit, while $(\rho_e)_B / \rho_e$ monotonically increases with B , eventually approaching the limiting linear trend. The combined result of the two effects is that λ_{eN} decreases with increasing B in weak field regime, and starts to increase in strong field regime after some turn-over point. From dimensional analysis, we expect the field at the turn-over point to be $B_c \sim E_{\text{eff}}^2 / e$ with E_{eff} being some typical energy of the particles participating in the reaction. Because of the threshold, e^- participating in $e^- + p \rightarrow \nu_e + n$ is more energetic than e^+ in $e^+ + n \rightarrow \bar{\nu}_e + p$. So B_c is larger for panels (a) and (c) than for panels (b) and (d), respectively, in Fig. 3. The turn-over points correspond to $B_c \sim 2 \times 10^{15}$ G in panel (b) and $B_c < 10^{15}$ G in panel (d). However, the turn-over in these two panels is much weaker than that in panels (a) and (c) so that $\lambda_{e+n}^{(0,B)}$ and $\lambda_{e+n}^{(1,B)}$ appear to increase monotonically with B for $B \gtrsim 10^{15}$ G. In addition, because E_{eff} is higher for higher T , B_c is larger for panels (a) and (b) ($T = 2$ MeV) than for panels (c) and (d) ($T = 1$ MeV) in Fig. 3.

In summary, we note that the rates λ_{eN} are sensitive to the temperature T of the supernova environment regardless of B : lowering T by a factor of two reduces λ_{e-p} by factors of $\sim 30-50$ and λ_{e+n} by factors of $\sim 6-20$ (see Fig. 3). In contrast, the average cross sections $\langle \sigma_{\nu N} \rangle$ only have minor dependence on T (mainly through the polarization of nucleon spin) so that the rates $\lambda_{\nu N}$ essentially scale with the radius R as $\lambda_{\nu N} \propto R^{-2}$. For the temperature profile in the supernova environment of interest, the rates $\lambda_{\nu N}$ dominate λ_{eN} . Therefore, so long as the former rates are calculated accurately, the latter can be estimated using $\lambda_{eN}^{(0,B)}$ to good approximation for $B \lesssim 10^{16}$ G.

V. CONCLUSIONS

We have developed a numerical method for calculating to $\mathcal{O}(1/m_N)$ the rates of $\nu_e + n \rightleftharpoons e^- + p$ and $\bar{\nu}_e + p \rightleftharpoons e^+ + n$ in supernova environments with strong magnetic fields. We have shown that our results have the correct behavior in the limit of high neutrino energy or small magnetic field. We find that for typical supernova ν_e energy distributions, magnetic fields of $B \sim 10^{16}$ G reduce the rate of $\nu_e + n \rightarrow e^- + p$ while the $\mathcal{O}(1/m_N)$ corrections due to weak magnetism and nucleon recoil increase this rate. These two opposite effects tend to cancel. On the other hand, the reduction of the rate of $\bar{\nu}_e + p \rightarrow e^+ + n$ by the $\mathcal{O}(1/m_N)$ corrections dominates the magnetic field effects for $B \lesssim 10^{16}$ G and typical supernova $\bar{\nu}_e$ energy distributions. We also find that for typical supernova conditions relevant for heavy element nucleosynthesis, the rates of $e^- + p \rightarrow \nu_e + n$ and $e^+ + n \rightarrow \bar{\nu}_e + p$ first decrease and then increase with increasing B . As it is extremely time consuming to numerically calculate to $\mathcal{O}(1/m_N)$ the rates for the above processes in strong magnetic fields, we recommend that for $B \lesssim 10^{16}$ G, the following approximations be implemented in models of supernova nucleosynthesis. For $\nu_e + n \rightarrow e^- + p$, it is simple to calculate the average cross section including the magnetic field effects but no $\mathcal{O}(1/m_N)$ corrections [$\langle \sigma_{\nu_e n}^{(0,B)} \rangle$ in Table I] or vice versa [$\langle \sigma_{\nu_e n}^{(1)} \rangle$ in Table I]. By comparing the two with $\langle \sigma_{\nu_e n}^{(0)} \rangle$, one can estimate the effects of magnetic fields and the $\mathcal{O}(1/m_N)$ corrections, respectively. With these two kinds of corrections combined, $\langle \sigma_{\nu_e n}^{(1)} \rangle + [\langle \sigma_{\nu_e n}^{(0,B)} \rangle - \langle \sigma_{\nu_e n}^{(0)} \rangle]$ agrees with the result of the full calculation at the level of $\sim 1\%$. For $\bar{\nu}_e + p \rightarrow e^+ + n$, the magnetic field effects on the average cross section can be ignored but the $\mathcal{O}(1/m_N)$ corrections should be included with an exact treatment of the reaction kinematics [$\langle \sigma_{\bar{\nu}_e p}^{(1*)} \rangle$ in Table I]. For $e^- + p \rightarrow \nu_e + n$ and $e^+ + n \rightarrow \bar{\nu}_e + p$, the rates including the magnetic field effects but no $\mathcal{O}(1/m_N)$ corrections [Eqs. (69)–(71)] are sufficient.

Acknowledgments

We would like to thank Arkady Vainshtein for helpful discussions. We also want to thank John Beacom for communications regarding the effects of weak magnetism and nucleon recoil on neutrino processes. This work was supported in part by DOE grant DE-FG02-87ER40328.

APPENDIX A: SPECIAL FUNCTION

The special function $I_{n,r}(\zeta)$ can be written as [18]

$$I_{n,r}(\zeta) = \sqrt{\frac{r!}{n!}} e^{-\zeta/2} \zeta^{(n-r)/2} L_r^{n-r}(\zeta), \quad (\text{A1})$$

where $L_n^\alpha(x)$ is the generalized Laguerre polynomial defined as [17]

$$L_n^\alpha(x) = \frac{1}{n!} e^x x^{-\alpha} \frac{d^n}{dx^n} (e^{-x} x^{n+\alpha}) \quad (\text{A2a})$$

$$= \sum_{m=0}^n (-1)^m \binom{n+\alpha}{n-m} \frac{x^m}{m!}. \quad (\text{A2b})$$

To calculate $I_{n,r}(\zeta)$ efficiently, we use its properties given below.

- *Mirror relation*

Based on the identity [12]

$$(-1)^{n-r} \zeta^{-(n-r)} Q_n^{r-n}(\zeta) = Q_r^{n-r}(\zeta), \quad (\text{A3})$$

where

$$Q_r^{n-r}(\zeta) \equiv r! L_r^{n-r}(\zeta), \quad (\text{A4})$$

it is straightforward to show that

$$I_{n,r}(\zeta) = (-1)^{n-r} I_{r,n}(\zeta). \quad (\text{A5})$$

- *Recursion relations*

Using the recursion relation of the generalized Laguerre polynomial [17]

$$L_n^{\alpha-1}(\zeta) = L_n^\alpha(\zeta) - L_{n-1}^\alpha(\zeta), \quad (\text{A6})$$

one can show that

$$\begin{aligned} I_{n,r}(\zeta) &= \sqrt{\frac{r!}{n!}} e^{-\zeta/2} \zeta^{(n-r)/2} L_r^{n-r}(\zeta) \left[L_r^{(n-1)-r}(\zeta) + L_{r-1}^{(n-1)-(r-1)}(\zeta) \right] \\ &= \sqrt{\frac{\zeta}{n}} I_{n-1,r}(\zeta) + \sqrt{\frac{r}{n}} I_{n-1,r-1}(\zeta). \end{aligned} \quad (\text{A7})$$

Using this recursion relation and the mirror relation in Eq. (A5), one can prove another recursion relation

$$I_{n,r}(\zeta) = -\sqrt{\frac{\zeta}{r}} I_{n,r-1}(\zeta) + \sqrt{\frac{n}{r}} I_{n-1,r-1}(\zeta). \quad (\text{A8})$$

Starting from the definition

$$I_{0,0}(\zeta) = e^{-\zeta/2}, \quad (\text{A9})$$

one can use the recursion relation in Eq. (A7) to obtain

$$I_{n,0}(\zeta) = \sqrt{\frac{\zeta^n}{n!}} I_{0,0}(\zeta). \quad (\text{A10})$$

Using the above result and the mirror relation in Eq. (A5), one has

$$I_{0,r}(\zeta) = (-1)^r \sqrt{\frac{\zeta^n}{r!}} I_{0,0}(\zeta). \quad (\text{A11})$$

The function $I_{n,r}(\zeta)$ with $n > 0$ and $r > 0$ can be calculated as follows:

1. Compute $I_{n-1,0}(\zeta)$ and $I_{n,0}(\zeta)$ from Eq. (A10). Set $r' = 1$.
2. Compute $I_{n,r'}(\zeta)$ from the recursion relation in Eq. (A8).
3. If $r' = r$, finish. Otherwise, compute $I_{n-1,r'}(\zeta)$ from the recursion relation in Eq. (A7).
4. Advance r' by unity and return to step 2.

APPENDIX B: REDUCED AMPLITUDE SQUARED

The reduced amplitude squared $\mathcal{W}_{\nu_e n}$ for $\nu_e + n \rightarrow e^- + p$ is defined in Eq. (39). The amplitude $\mathfrak{M}_{\nu_e n}$ [Eq. (33)] contained in $\mathcal{W}_{\nu_e n}$ can be simplified using

$$\begin{aligned} & \int_0^\infty \xi d\xi \int_0^{2\pi} e^{i\mathbf{w}_\perp \cdot \mathbf{x}_\perp - i(n_e - r_e - n_p + r_p)\phi} I_{n_p, r_p}(eB\xi^2/2) I_{n_e, r_e}(eB\xi^2/2) d\phi \\ &= \frac{2\pi}{eB} i^{(n_e - r_e - n_p + r_p)} e^{-i(n_e - r_e - n_p + r_p)\phi_w} I_{n_e, n_p}(w_\perp^2/2eB) I_{r_e, r_p}(w_\perp^2/2eB), \end{aligned} \quad (B1)$$

where ϕ_w is the azimuthal angle of \mathbf{w}_\perp . The above result follows from [5, 12, 17]

$$\int_0^{2\pi} e^{i\mathbf{w}_\perp \cdot \mathbf{x}_\perp - i(n-r)\phi} d\phi = 2\pi i^{n-r} e^{-i(n-r)\phi_w} J_{n-r}(w_\perp \xi) \quad (B2)$$

and

$$\int_0^\infty J_{(n-r)-(n'-r')}(2\sqrt{u\zeta}) I_{n', r'}(u) I_{n, r}(u) du = I_{n, n'}(\zeta) I_{r, r'}(\zeta), \quad (B3)$$

where $J_n(\zeta)$ is the Bessel function.

Noting that [12]

$$\sum_r I_{n, r}(\zeta) I_{n', r}(\zeta) = \delta_{n, n'} \quad (B4)$$

and using Eqs. (11) and (B1), we are able to derive the following explicit expressions of $\mathcal{W}_{\nu_e n}$ with the help of MATHMATICA[®]:

$$\begin{aligned} (\mathcal{W}_{\nu_e n})_{s_p=1, s_n=1} &= (f+g)^2(1+v_{ez})(1+\cos\Theta_\nu) I_{n_e, n_p}^2(w_\perp^2/2eB) \\ &+ (f-g)^2(1-v_{ez})(1-\cos\Theta_\nu) I_{n_e-1, n_p}^2(w_\perp^2/2eB) \\ &+ 2(f^2-g^2) \frac{\sqrt{2n_e eB}}{E_e} \cos\phi_w \sin\Theta_\nu I_{n_e-1, n_p}(w_\perp^2/2eB) I_{n_e, n_p}(w_\perp^2/2eB) \\ &+ \frac{1}{m_N} \left\{ \left[-(f+g)^2(1+v_{ez})(1+\cos\Theta_\nu)(k_{nz} + k_{pz}) \right. \right. \\ &\quad - (f+g)(2f+f_2)(1+v_{ez}) \sin\Theta_\nu k_{nx} \\ &\quad + f_2(f+g)(1+v_{ez}) \sin\Theta_\nu w_x \\ &\quad + (f+g)(2f+f_2)(1+\cos\Theta_\nu) \frac{2n_e eB}{E_e} \left. \right] \times I_{n_e, n_p}^2(w_\perp^2/2eB) \\ &+ \left[(f-g)^2(1-v_{ez})(1-\cos\Theta_\nu)(k_{nz} + k_{pz}) \right. \\ &\quad + f_2(f-g)(1-v_{ez}) \sin\Theta_\nu k_{nx} \\ &\quad - (f-g)(2f+f_2)(1-v_{ez}) \sin\Theta_\nu w_x \\ &\quad - f_2(f-g)(1-\cos\Theta_\nu) \frac{2n_e eB}{E_e} \left. \right] \times I_{n_e-1, n_p}^2(w_\perp^2/2eB) \\ &+ \left[-f_2(f+g)(1+v_{ez}) \sin\Theta_\nu \cos\phi_w \sqrt{2n_e eB} \right. \\ &\quad + (f-g)(2f+f_2)(1-v_{ez}) \sin\Theta_\nu \cos\phi_w \sqrt{2n_e eB} \\ &\quad + 2(-f^2+g(f+f_2) + f(f-g+f_2) \cos\Theta_\nu) \\ &\quad \times \cos(\Phi_n - \phi_w) \frac{\sqrt{2n_e eB} k_{n\perp}}{E_e} \\ &\quad - (f+g)(2f+f_2)(1+\cos\Theta_\nu) \frac{\sqrt{2n_e eB} w_\perp}{E_e} \\ &\quad \left. \left. + f_2(f-g)(1-\cos\Theta_\nu) \frac{\sqrt{2n_e eB} w_\perp}{E_e} \right] \right\} \end{aligned}$$

$$\times I_{n_e-1, n_p}(w_\perp^2/2eB) I_{n_e, n_p}(w_\perp^2/2eB) \Big\}, \quad (B5a)$$

$$\begin{aligned} (\mathcal{W}_{\nu_e n})_{s_p=1, s_n=-1} = & 4g^2(1+v_{ez})(1-\cos\Theta_\nu)I_{n_e, n_p}^2(w_\perp^2/2eB) \\ & + \frac{2}{m_N} \left\{ \left[-g(f+g+f_2)(1+v_{ez})\sin\Theta_\nu k_{nx} \right. \right. \\ & \quad + 2g(f+f_2)(1+v_{ez})(1-\cos\Theta_\nu)(k_{ez}-k_{\nu z}) \\ & \quad + g(f+g+f_2)(1-\cos\Theta_\nu) \frac{2n_e e B}{E_e} \Big] \times I_{n_e, n_p}^2(w_\perp^2/2eB) \\ & \quad + g(f-g+f_2)(1+v_{ez})\sin\Theta_\nu w_x I_{n_e, n_p-1}^2(w_\perp^2/2eB) \\ & \quad \left. \left. + \left[g(f-g+f_2)k_{n\perp} \cos(\Phi_n - \phi_w) - g(f+g+f_2)w_\perp \right] \right. \right. \\ & \quad \times (1-\cos\Theta_\nu) \frac{\sqrt{2n_e e B}}{E_e} I_{n_e-1, n_p}(w_\perp^2/2eB) I_{n_e, n_p}(w_\perp^2/2eB) \\ & \quad - g(f-g+f_2)(1+v_{ez})\sin\Theta_\nu \cos\phi_w \sqrt{2n_e e B} \\ & \quad \left. \times I_{n_e-1, n_p-1}(w_\perp^2/2eB) I_{n_e, n_p-1}(w_\perp^2/2eB) \right\}, \end{aligned} \quad (B5b)$$

$$\begin{aligned} (\mathcal{W}_{\nu_e n})_{s_p=-1, s_n=1} = & 4g^2(1-v_{ez})(1+\cos\Theta_\nu)I_{n_e-1, n_p-1}^2(w_\perp^2/2eB) \\ & + \frac{2}{m_N} \left\{ \left[-g(f+g+f_2)(1-v_{ez})\sin\Theta_\nu k_{nx} \right. \right. \\ & \quad - 2g(f+f_2)(1-v_{ez})(1+\cos\Theta_\nu)(k_{ez}-k_{\nu z}) \\ & \quad + g(f+g+f_2)(1+\cos\Theta_\nu) \frac{2n_e e B}{E_e} \Big] \times I_{n_e-1, n_p-1}^2(w_\perp^2/2eB) \\ & \quad + g(f-g+f_2)(1-v_{ez})\sin\Theta_\nu w_x I_{n_e-1, n_p}^2(w_\perp^2/2eB) \\ & \quad \left. \left. + \left[g(f-g+f_2)k_{n\perp} \cos(\Phi_n - \phi_w) - g(f+g+f_2)w_\perp \right] \right. \right. \\ & \quad \times (1+\cos\Theta_\nu) \frac{\sqrt{2n_e e B}}{E_e} I_{n_e-1, n_p-1}(w_\perp^2/2eB) I_{n_e, n_p-1}(w_\perp^2/2eB) \\ & \quad - g(f-g+f_2)(1-v_{ez})\sin\Theta_\nu \cos\phi_w \sqrt{2n_e e B} \\ & \quad \left. \times I_{n_e-1, n_p}(w_\perp^2/2eB) I_{n_e, n_p}(w_\perp^2/2eB) \right\}, \end{aligned} \quad (B5c)$$

$$\begin{aligned} (\mathcal{W}_{\nu_e n})_{s_p=-1, s_n=-1} = & (f+g)^2(1-v_{ez})(1-\cos\Theta_\nu)I_{n_e-1, n_p-1}^2(w_\perp^2/2eB) \\ & + (f-g)^2(1+v_{ez})(1+\cos\Theta_\nu)I_{n_e, n_p-1}^2(w_\perp^2/2eB) \\ & + 2(f^2-g^2) \frac{\sqrt{2n_e e B}}{E_e} \cos\phi_w \sin\Theta_\nu I_{n_e-1, n_p-1}(w_\perp^2/2eB) I_{n_e, n_p-1}(w_\perp^2/2eB) \\ & + \frac{1}{m_N} \left\{ \left[(f+g)^2(1-v_{ez})(1-\cos\Theta_\nu)(k_{nz}+k_{pz}) \right. \right. \\ & \quad - (f+g)(2f+f_2)(1-v_{ez})\sin\Theta_\nu k_{nx} \\ & \quad + f_2(f+g)(1-v_{ez})\sin\Theta_\nu w_x \\ & \quad + (f+g)(2f+f_2)(1-\cos\Theta_\nu) \frac{2n_e e B}{E_e} \Big] \times I_{n_e-1, n_p-1}^2(w_\perp^2/2eB) \\ & \quad + \left. \left. \left[- (f-g)^2(1+v_{ez})(1+\cos\Theta_\nu)(k_{nz}+k_{pz}) \right. \right. \right. \\ & \quad + f_2(f-g)(1+v_{ez})\sin\Theta_\nu k_{nx} \\ & \quad - (f-g)(2f+f_2)(1+v_{ez})\sin\Theta_\nu w_x \\ & \quad - f_2(f-g)(1+\cos\Theta_\nu) \frac{2n_e e B}{E_e} \Big] \times I_{n_e, n_p-1}^2(w_\perp^2/2eB) \\ & \quad + \left. \left. \left[- f_2(f+g)(1-v_{ez})\sin\Theta_\nu \cos\phi_w \sqrt{2n_e e B} \right. \right. \right. \end{aligned}$$

$$\begin{aligned}
& + (f - g)(2f + f_2)(1 + v_{ez}) \sin \Theta_\nu \cos \phi_w \sqrt{2n_e e B} \\
& - 2(f^2 - g(f + f_2) + f(f - g + f_2) \cos \Theta_\nu) \\
& \times \cos(\Phi_n - \phi_w) \frac{\sqrt{2n_e e B} k_{n\perp}}{E_e} \\
& - (f + g)(2f + f_2)(1 - \cos \Theta_\nu) \frac{\sqrt{2n_e e B} w_\perp}{E_e} \\
& + f_2(f - g)(1 + \cos \Theta_\nu) \frac{\sqrt{2n_e e B} w_\perp}{E_e} \\
& \times I_{n_e-1, n_p-1}(w_\perp^2/2eB) I_{n_e, n_p-1}(w_\perp^2/2eB) \Big\}. \tag{B5d}
\end{aligned}$$

In the above equations, $v_{ez} = k_{ez}/E_e$. The reduced amplitude squared $\mathcal{W}_{\bar{\nu}_e p}$ for $\bar{\nu}_e + p \rightarrow e^+ + n$ can be obtained from these equations by making the substitution given in Eq. (49).

-
- [1] H. A. Bethe and J. R. Wilson, *Astrophys. J.* **295**, 14 (1985).
[2] Y.-Z. Qian and S. E. Woosley, *Astrophys. J.* **471**, 331 (1996), astro-ph/9611094.
[3] S. E. Woosley and R. D. Hoffman, *Astrophys. J.* **395**, 202 (1992).
[4] R. D. Hoffman, S. E. Woosley, G. M. Fuller, and B. S. Meyer, *Astrophys. J.* **460**, 478 (1996).
[5] H. Duan and Y.-Z. Qian, *Phys. Rev.* **D69**, 123004 (2004), astro-ph/0401634.
[6] C. J. Horowitz, *Phys. Rev.* **D65**, 043001 (2002), astro-ph/0109209.
[7] C. Kouveliotou, T. Strohmayer, K. Hurley, J. van Paradijs, M. H. Finger, S. Dieters, P. Woods, C. Thompson, and R. C. Duncan, *Astrophys. J.* **510**, L115 (1999), astro-ph/9809140.
[8] E. V. Gotthelf, G. Vasisht, and T. Dotani, *Astrophys. J.* **522**, L49 (1999), astro-ph/9906122.
[9] A. I. Ibrahim, J. H. Swank, and W. Parke, *Astrophys. J.* **584**, L17 (2003), astro-ph/0210515.
[10] D. Lai, *Rev. Mod. Phys.* **73**, 629 (2001), astro-ph/0009333.
[11] L. D. Landau and E. M. Lifshitz, *Quantum Mechanics: Non-Relativistic Theory* (Butterworth-Heinemann, Oxford, 1977), 3rd ed.
[12] A. A. Sokolov and I. M. Temov, *Synchrotron Radiation* (Pergamon, Oxford, 1968).
[13] H. Duan, Ph.D. thesis, University of Minnesota (2004).
[14] P. Vogel and J. F. Beacom, *Phys. Rev.* **D60**, 053003 (1999), hep-ph/9903554.
[15] C. J. Horowitz and G. Li, *Phys. Rev. Lett.* **82**, 5198 (1999).
[16] A. Strumia and F. Vissani, *Phys. Lett.* **B564**, 42 (2003), astro-ph/0302055.
[17] I. S. Gradshteyn and I. M. Ryzhik, *Table of integrals, series and products* (Academic, New York, 1980).
[18] P. Arras and D. Lai, *Phys. Rev.* **D60**, 043001 (1999), astro-ph/9811371.